

Neon in ultrashort and intense x rays from free electron lasers

Christian Buth,^{1,*} Randolph Beerwerth,^{2,3} Razib Obaid,⁴
Nora Berrah,⁴ Lorenz S. Cederbaum,¹ and Stephan Fritzsche^{2,3}

¹*Theoretische Chemie, Physikalisch-Chemisches Institut,
Ruprecht-Karls-Universität Heidelberg, Im Neuenheimer Feld 229, 69120 Heidelberg, Germany*

²*Helmholtz-Institut Jena, Fröbelstieg 3, 07743 Jena, Germany*

³*Theoretisch-Physikalisches Institut, Friedrich-Schiller-Universität Jena, Max-Wien-Platz 1, 07743 Jena, Germany*

⁴*Department of Physics, University of Connecticut,
2152 Hillside Road, U-3046, Storrs, Connecticut 06269, USA*

(Dated: 22 May 2017)

We theoretically examine neon atoms in ultrashort and intense x rays from free electron lasers and compare our results with data from experiments conducted at the Linac Coherent Light Source (LCLS). For this purpose, we treat in detail the electronic structure in all possible non-relativistic cationic configurations using a relativistic multiconfiguration approach. The interaction with the x rays is described in rate-equation approximation. To understand the mechanisms of the interaction, a path analysis is devised which allows us to investigate what sequences of photoionization and decay processes lead to a specific configuration and with what probability. Thereby, we uncover a connection to the mathematics of graph theory and formal languages. In detail, we study the ion yields and find that plain rate equations do not provide a satisfactory description. We need to extend the rate equations for neon to incorporate double Auger decay of a K -shell vacancy and photoionization shake off for neutral neon. Shake off is included for valence and core ionization; the former has hitherto been overlooked but has important consequences for the ion yields from an x-ray energy below the core ionization threshold. Furthermore, we predict the photon yields from XUV and x-ray fluorescence; these allow one insights into the configurations populated by the interaction with the x rays. Finally, we discover that inaccuracies in those Auger decay widths employed in previous studies have only a minor influence on ion and photon yields.

Keywords: ultrashort and intense x rays, neon atom, multiconfiguration Dirac-Hartree-Fock, rate equations, free-electron laser, ion yield, photon yield

I. INTRODUCTION

Atoms are the basic constituents of aggregates of matter realized in molecules, clusters, and solids. In this way, the study of the interaction of intense and ultrafast x rays with atoms is of fundamental importance for all research involving matter in such light. Intense x rays offer manifold novel perspectives for science such as diffraction experiments with single molecules [1] and x-ray quantum optics [2].

Experimentally, research with intense and ultrafast x rays has only recently become a reality by the novel x-ray free electron lasers (FELs) of which there are presently four producing soft to hard x rays: the Linac Coherent Light Source (LCLS) [3, 4] in Menlo Park, California, USA, the SPring-8 Angstrom Compact free electron LAser (SACLA) [5] in Sayo-cho, Sayo-gun, Hyogo, Japan, the SwissFEL [6] in Villigen, Switzerland, and the European X-Ray Free-Electron Laser (XFEL) [7] in Hamburg, Germany.

The novel FEL facilities which produce x rays with unprecedented characteristics inspire one to investigate processes, known from the strong-field interaction of optical lasers with atoms, but with x rays that go be-

yond the well-established one-x-ray-photon science only possible at synchrotron light sources [8]. With x rays the sequential absorption of multiple photons [9–16] or the simultaneous absorption of two photons [17, 18] are the possible processes. Even Rabi flopping [19–21] on x-ray transitions becomes feasible. The FEL can be used to pump x-ray lasing [22, 23] on an inner-shell atomic transition which can be controlled by an additional optical laser [24]. But the two-color physics of FEL x rays and an optical laser offers even more promising avenues: high-order harmonic generation becomes feasible in the kilo-electronvolt regime [25–28] and high-energy frequency combs [29, 30] can be produced.

Neon has been studied extensively in LCLS radiation both experimentally [12, 17, 31] and theoretically [32–37]. The quantum dynamics of neon atoms in intense and ultrashort x-ray radiation was initially described theoretically with a plain rate-equation model [12, 32, 33] that considered only one-photon cross sections and radiative and Auger decay widths. The model worked well for a photon energy of 800 eV below the K -shell ionization threshold where it seemingly correctly predicted the ion yields [12]. This view did not change in a careful reinvestigation of neon in this case using master equations [36]. Yet the model failed to adequately describe ion yields for photon energies above the K -shell ionization threshold. Subsequent theoretical research [17, 34, 35] revealed that there are substantial further many-electron effects in

* World Wide Web: www.christianbuth.name, electronic mail; christian.buth@web.de

neon in this case. Specifically, shake off following K -shell ionization [17] and double Auger decay of a K -shell vacancy [35] were included in extended rate-equation models for neon. This mitigated substantially the discrepancy found between the ion yields from the experiment and the plain rate equations. But this was not the only shortcoming of the initial theoretical description [32]. Already in Ref. 17 a remaining discrepancy between the experimental and the theoretical ion yields was conjectured to be due to resonant excitations. Such inner-shell resonant absorption [34] was found to be essential to understand the interaction of neon with 1050 eV x rays.

Yet there are still gaps in our understanding of the interaction of even one of the simplest atoms with intense and ultrafast x rays left. A detailed knowledge of the electronic structure of atoms is the basis for an understanding of experiments at x-ray FELs. After the systematic study of neon in all cationic charge states of Ref. 38 in the year 1973 with the Hartree-Fock-Slater approximation, little has been done with modern atomic theory. On the contrary, the description of the electronic structure in intense x-ray-atom interaction is frequently still in Hartree-Fock-Slater [32, 39] or Dirac-Hartree-Slater [13, 15, 16] approximation.

This article is structured as follows. We use state of the art atomic electronic structure theory discussed in section II. Based on it, a description of the x-ray interaction with neon is developed in section III first with the photoionization cross sections and Auger and radiative decay widths and, second, including two-electron emission by photoionization shake off for neutral neon and double Auger decay of a K -shell vacancy in Ne^+ . To understand the involved processes in the rate equations more deeply than with an analysis only of the Auger electron yield used previously [12, 32], we devise a path analysis in section IV. Ion yields are calculated in section V and compared with experimental data. The XUV and x-ray photon yields of neon are predicted in section VI. Finally, computational details are given in section VII and conclusions are drawn in section VIII.

Equations are formulated in atomic units [40, 41]. Details of the calculations in this article are provided in the Supplementary Data [42].

II. ATOMIC ELECTRONIC STRUCTURE OF MULTIPLY-IONIZED NEON

A. Relativistic multiconfiguration approach

We pursue quite accurate electronic structure calculations with state-of-the-art atomic theory [44, 45]. This avails detailed fine-structure-resolved information. Yet, nonetheless, we make the configuration approximation for the atomic structure to simplify the description. This refers to Hartree-Fock-Slater theory in which the configurations of neon $1s^\ell 2s^m 2p^n$ with $\ell, m, n \in \mathbb{N}_0 \wedge \ell, m \leq 2 \wedge n \leq 6$ are the actual electronic states [38, 45]. In

other words, we probabilistically average the over the fine-structure resolved results to obtain configuration-averaged quantities. These are the only ones that are used in the subsequently.

To understand the electronic structure of the atom and photoionization, electronic, and radiative transitions in all cationic charge states, the cationic configurations are generated starting from the neutral atom by systematically removing electrons. We frequently abbreviate these configurations by their occupation numbers, i.e., for neon in $1s^\ell 2s^m 2p^n$, we simply write ℓmn . As we consider only cationic configurations, the occupation numbers are, thereby, restricted to the maximum number found for the ground state of the atom, i.e., the configurations of neon form the set

$$\mathbb{K} = \{\ell mn \mid \ell, m, n \in \mathbb{N}_0 \wedge \ell, m \leq 2 \wedge n \leq 6\}. \quad (1)$$

We use GRASP2K (General-purpose Relativistic Atomic Structure Program) [46, 47] to perform multiconfiguration Dirac-Hartree-Fock (MCDHF) computations for all $i \in \mathbb{K} \wedge i \neq 000$. Typically, such a calculation is carried out for each single nonrelativistic configuration $1s^\ell 2s^m 2p^n$. However, if $\ell = m = 1$, MCDHF does not converge due to orbital rotations [45] unless the de-excited configuration $1s^2 2s^0 2p^n$ is included as well.

Based on the relativistic electronic structure, transitions can be determined with RATIP (Relativistic Atomic Transition and Ionization Properties) [48]. Specifically, we compute photoionization, electronic, and radiative transitions. Thereby, individual electronic structure computations for the initial and final configurations are used. Unfortunately, RATIP cannot calculate photoionization cross sections for a hydrogen-like ion. Thus, we switch to FAC (Flexible Atomic Code) [49] in this case.

To make the configuration approximation for energies, widths, and cross sections, we note that GRASP2K [46, 47] and RATIP [48] both are fully relativistic and fine-structure-resolved results are obtained. That means that a nonrelativistic configuration $c \in \mathbb{K} \wedge c \neq 000$ does not usually correspond to a single state but to a number of states N_c , i.e., the multiplet, which are indexed in terms of the set $\mathbb{M}_c = \{1, \dots, N_c\}$. Therefore, a probabilistic average over the states in a multiplet is required for the quantities of interest in configuration approximation. To carry out this average, a probabilistic occupation of the states in the multiplet is *assumed* [50], i.e., every state is occupied with the same probability; thereby, we need to account for the fact that state $\alpha \in \mathbb{M}_c$ is $(2J_\alpha + 1)$ fold degenerate with its total angular momentum J_α . We find the average energy of a multiplet, i.e., the energy of the configuration $c \in \mathbb{K} \wedge c \neq 000$, to be

$$E_{C,c} = \frac{1}{S_c} \sum_{\alpha \in \mathbb{M}_c} (2J_\alpha + 1) E_\alpha, \quad (2)$$

where E_α is the energy of the state $\alpha \in \mathbb{M}_c$. The sum of the probabilistic factors is $S_c = \sum_{\alpha \in \mathbb{M}_c} (2J_\alpha + 1)$. For the electron-bare nucleus, we have $\mathbb{M}_{000} = \emptyset$ and $E_{C,000} = 0$.

To select electronic transitions and calculate transition energies and decay widths, we need to identify potential electronic decay channels. Thereby, lower subshell and upper subshell refer to electron subshells which have an energy that is lower for the lower subshell and higher for the upper subshell. A pair of configurations is connected by an electronic decay, if

- (a) the final configuration has a lower subshell with an electron more than the initial configuration,
- (b) the final configuration has two electrons less either in one upper subshell or distributed over two upper subshells than the initial configuration, and
- (c) all other subshells of the initial and the final configurations are occupied the same.

For each pair of configurations for which electronic transitions occur there are initial states derived from the initial configuration $i \in \mathbb{K}$ with a higher energy than, at least one, final state derived from the final configuration $f \in \mathbb{K}$, i.e., that the maximum value of the energies of the initial-state multiplet is larger than the minimum value of the final-state multiplet. We sum over the difference of all such pairs of initial- and final-state energies weighted by probabilistic factors yielding the transition energy in configuration approximation

$$E_{E,f \leftarrow i} = \frac{1}{S'_i} \sum_{\substack{\alpha \in \mathbb{M}_i \\ S'_{f\alpha} \neq 0}} (2J_\alpha + 1) \left[E_\alpha - \frac{1}{S''_{f\alpha}} \sum_{\substack{\beta \in \mathbb{M}_f \\ E_\beta < E_\alpha}} (2J_\beta + 1) E_\beta \right] \quad (3)$$

The sum of the probabilistic factors of the states of the final configuration f depending on the initial state α is $S''_{f\alpha} = \sum_{\substack{\beta \in \mathbb{M}_f \\ E_\beta < E_\alpha}} (2J_\beta + 1)$; it is zero, if no final states

are reachable from β by electronic decay. The sum of the probabilistic factors for the initial configuration i is given by $S'_i = \sum_{\substack{\alpha \in \mathbb{M}_i \\ S'_{f\alpha} \neq 0}} (2J_\alpha + 1)$. Equation (3) ap-

pears more complicated than it should be at first sight. Naively, we expect that $E_{E,f \leftarrow i}$ is simply given by the difference $E_{C,f} - E_{C,i}$ of the average energies of the final and initial configurations (2). In fact, Equation (3) reduces to this case for non-overlapping multiplets of the initial and final configuration, i.e., $\max_{\beta \in \mathbb{M}_f} E_\beta < \min_{\alpha \in \mathbb{M}_i} E_\alpha$.

However, for overlapping multiplets, not all initial states undergo transitions to all final states. Thus we need to pick out those transitions which actually occur and take only those into account in the probabilistic average (3). To determine the electronic decay width $\Gamma_{E,f \leftarrow i}$ in configuration approximation, we probabilistically average over the electronic decay widths of the states

$$\Gamma_{E,f \leftarrow i} = \frac{1}{S_i} \sum_{\alpha \in \mathbb{M}_i} (2J_\alpha + 1) \sum_{\substack{\beta \in \mathbb{M}_f \\ E_\alpha > E_\beta}} \gamma_{E,\beta \leftarrow \alpha} \quad (4)$$

Here $\gamma_{E,\beta \leftarrow \alpha}$ is the decay width from the state α to β .

Radiative transitions occur between (some of) the states in the multiplets associated with a pair of configurations, if

- (a) the final configuration has a lower subshell with an electron more than the initial configuration,
- (b) the final configuration has an electrons less in an upper subshell than the initial configuration, and
- (c) all other subshells of the initial and the final configurations are occupied the same.

Then there are initial states with a higher energy than the final states and radiative transitions occur. All said for electronic transition energies $E_{R,f \leftarrow i}$ applies also for radiative transition energies and we use (3). Radiative decay widths $\Gamma_{R,f \leftarrow i}$ are obtained analogously to (4).

Photoionization also involves a pair of configurations chosen as follows

- (a) the final configuration has a subshell with an electron less than the initial configuration, and
- (b) all other subshells of the initial and the final configurations are occupied the same.

Photoionization may occur if there are initial states with a lower energy than the final states. The minimum photon energy required to ionize the atom in the initial configuration is the threshold ionization energy; it is given by

$$E_{P,f \leftarrow i} = \min_{\substack{\alpha \in \mathbb{M}_i, \beta \in \mathbb{M}_f \\ E_\beta > E_\alpha}} (E_\beta - E_\alpha) \quad (5)$$

This expression works also for overlapping initial and final state multiplets because we require that $E_\beta > E_\alpha$ in the minimization which picks out only pairs of initial and final states that can be connected by photoionization. The probabilistic average of the cross section for $f \neq 000$ is

$$\sigma_{f \leftarrow i} = \frac{1}{S'_i} \sum_{\alpha \in \mathbb{M}_i} (2J_\alpha + 1) \sum_{\substack{\beta \in \mathbb{M}_f \\ E_\beta > E_\alpha}} \varsigma_{\beta \leftarrow \alpha} \quad (6)$$

where $\varsigma_{\beta \leftarrow \alpha}$ is the photoionization cross section for a transition from α to β . An empty sum in (6) is zero. The sum over the probabilistic factors is $S'_i = \sum_{\substack{\alpha \in \mathbb{M}_i \\ \exists \beta \in \mathbb{M}_f, E_\beta > E_\alpha}} (2J_\alpha + 1)$. For $f = 000$, we have $\sigma_{000 \leftarrow i} = \frac{1}{S_i} \sum_{\alpha \in \mathbb{M}_i} (2J_\alpha + 1) \varsigma_{0 \leftarrow \alpha}$ where $\varsigma_{0 \leftarrow \alpha}$ stands for the cross section to ionize the last electron of the atom in state α . Here and throughout we suppress in the notation the explicit dependence of the cross sections on the photon energy.

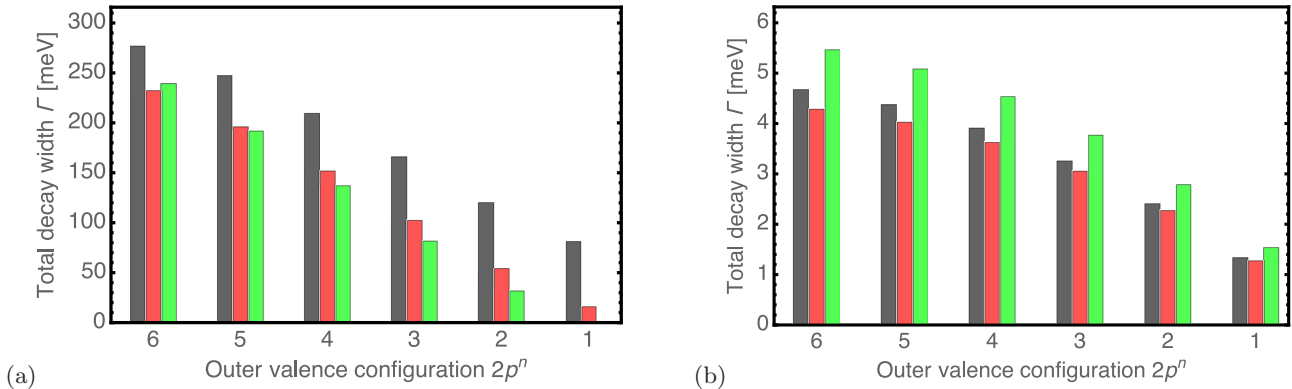


FIG. 1. (Color online) Total decay widths of single core holes in neon: (a) Auger widths and (b) radiative widths. The grey bars stand for the decay of the configurations $1s^1 2s^2 2p^n$, red bars for $1s^1 2s^1 2p^n$, and green bars for $1s^1 2s^0 2p^n$ with $n \in \{1, \dots, 6\}$.

B. Multiply-charged neon atoms

A neutral neon atom has 10 electrons; a total of 63 non-relativistic cationic configurations among which 68 Auger transitions and 100 radiative transitions occur; there are 138 one-photon ionization cross sections [42].

In figure 1, we depict the total Auger and radiative decay widths of single core holes in neon. For both, we observe a decreasing width with decreasing number of $2p$ electrons as there are fewer and fewer electrons available to make a transition. The largest Auger width, in figure 1(a), is found for 126, i.e., if all decay channels are present. However, the largest radiative width, in figure 1(b), occurs for the decay of 106, i.e., if both $2s$ electrons are missing due to a spatially more compact trication with a resulting larger dipole transition matrix elements involving the vacancy in the $1s$ shell and the $2p$ subshell. Similar trends arise for double core holes [42].

To assess the accuracy of our atomic data for neon, we compare it to the early calculations in Ref. 38 where the Hartree-Fock-Slater (HFS) approximation was used to represent the atomic electronic structure (for details see Ref. 42). The relative error of decay widths is expressed as

$$\frac{\Delta\Gamma}{\Gamma_{\text{rel}}} = \frac{\Gamma_{\text{rel}} - \Gamma_{\text{HFS}}}{\Gamma_{\text{rel}}}, \quad (7)$$

where Γ_{rel} stands for widths from RATIP [48] [Eq. (4)] and Γ_{HFS} are from Ref. 38. The relative error of total radiative decay widths is found to be generally smaller for double core holes, compared with single core holes. The reason is electron correlations in the K shell for single core holes which are not captured by the Hartree-Fock-Slater approximation. We find the same trend for the relative errors of the total Auger decay widths. Also we observe that partial and total Auger decay widths from RATIP [Eq. (4)] are always larger than those from Ref. 38. The relative error in the transition energies is small for radiative transitions where it is in most cases

smaller for double core holes compared with single core holes. The reverse trend is found for Auger transitions: energies for double core hole decay are overall less accurate than for single core hole decay. Frequently Auger transition energies have a larger relative error than radiative transitions energies.

III. X-RAY INTERACTION WITH NEON ATOMS

The cationic configurations of neon and photoionization, Auger, and radiative transitions among them, as debated in section II, can be visualized in a graph [51], figure 2; yet this gives only a static, time-independent view on the interaction with x rays. To gain insights into the time-dependent quantum dynamics of the absorption of x rays and the resulting decay processes, we employ the rate-equation approximation [13, 15, 16, 32, 39] that has been used successfully in a number of studies to describe experiments, e.g., Refs. 9, 12, 13, 15, 17, 31, 33–36. Exemplary rate equations for a nitrogen atom restricted to K -shell electrons are given in Ref. 13 and the formal structure of such rate equations is discussed in Ref. 16. Using rate equations implies that coherences are not included in the description. This is typically a good approximation for nonresonant absorption of x rays. However, if the x-ray energy is tuned to a resonance, then coherences manifest [2, 19–21, 29, 30, 36].

A. Plain rate equations

We formulate a system of rate equations, to which we refer as plain rate equations, using the configurations of neon (1) and the transitions among them determined in section II. The rate equations are expressed succinctly

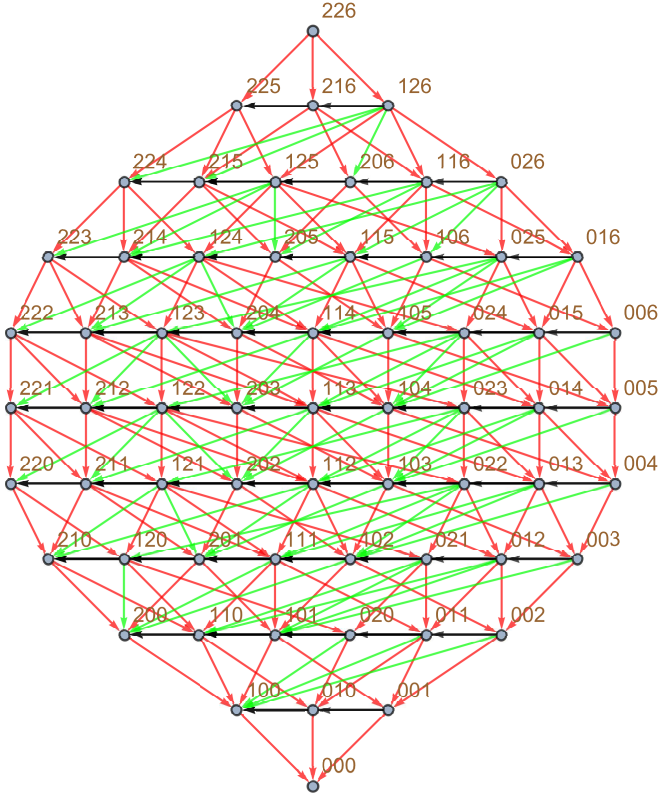


FIG. 2. (Color online) Graph of the configurations of neon and transitions among them. Configurations $1s^\ell 2s^m 2p^n$ are given by their occupation numbers ℓmn . **Red** arrows depict photoionization, **green** arrows Auger decay, and **black** arrows radiative transitions.

for $j \in \mathbb{K}$ as follows

$$\begin{aligned} \frac{dP_j(t)}{dt} = & \left[\sum_{i \in \mathbb{K}} \sigma_{j \leftarrow i} P_i(t) - \sigma_j P_j(t) \right] J_X(t) \\ & + \sum_{i \in \mathbb{K}} (\Gamma_{E,j \leftarrow i} + \Gamma_{R,j \leftarrow i}) P_i(t) \\ & - (\Gamma_{E,j} + \Gamma_{R,j}) P_j(t), \end{aligned} \quad (8)$$

where the partial cross sections are $\sigma_{j \leftarrow i}$ and their sum over j for a fixed i , the total cross section, is σ_i . The partial decay widths for Auger decay are $\Gamma_{E,j \leftarrow i}$ and for radiative decay are $\Gamma_{R,j \leftarrow i}$ where their sums over j for a fixed i are the total Auger and radiative decay widths $\Gamma_{E,i}$ and $\Gamma_{R,i}$, respectively. Note that the cross sections and the decay widths are only nonzero, if there are accessible final configurations. The x-ray pulse is quantified in (8) by its photon flux $J_X(t)$. The initial condition at $t \rightarrow \infty$ is that the neutral atom is in its ground state. In Eq. (8), we suppressed the spatial coordinates for the probabilities and the photon flux for clarity which we do

also in what follows (see section VII for details).

B. Two-electron emission in the rate equations

There are substantial many-electron effects in neon that are not captured by the cross sections and Auger decay widths considered so far in the rate equations (8). A lot of effort has gone into investigating such many-electron effects in neutral neon and singly ionized neon manifesting themselves as photoionization shake off and double Auger decay, respectively. However, information about such two-electron emission in higher-charged neon cations is missing. Specifically photoionization shake off can be expected to be significant still for Ne^+ because of its large contribution in neutral neon. However, generally, two-electron emission should become less important the more highly charged the cation becomes as the ionization threshold for liberating an additional electron moves considerably upward in energy [42]. In consequence, we extend the plain rate equations from section III A using the experimental results from Refs. 52–54 to include photoionization shake off and double Auger decay.

1. Modified rate equations due to photoionization shake off

For a photon energy larger than about 1050 eV—well above the double ionization threshold for a K -shell electron and a valence electron—photoionization shake off is saturated [52]. Then the number of doubly charged atoms produced by photoionization—for which not only the K -shell electron is ejected but, additionally, a valence electron leaves the atom—is 23% of the number of atoms produced with a single K vacancies [table III of Ref. 52]. For photon energies just above the neon K edge, this percentage varies, however, as, e.g., there is insufficient energy to eject a valence electron from the $2s$ subshell or at all. This can be disregarded in what follows because the photon energy is always much larger than the neon K edge or below it. We need to relate this experimental ratio of double ionization to single ionization $r_{1sL/1s} = 0.23$ to the core-ionization cross section $\sigma_{126 \leftarrow 226}$ which already is in the plain rate equations (8). For this purpose, we assume that $\sigma_{126 \leftarrow 226}$ provides the total amount of K vacancies formed which needs to be corrected for shake off, i.e., the contribution of single ionization is calculated with $(1 - s_C) \sigma_{126 \leftarrow 226}$ and the contribution of double ionization follows from $s_C \sigma_{126 \leftarrow 226}$ where s_C obeys $\frac{s_C}{1-s_C} = r_{1sL/1s} \Leftrightarrow s_C = \frac{r_{1sL/1s}}{1+r_{1sL/1s}}$. Furthermore, we assume that only a $2p$ electron is ejected by shake off. The plain rate equations are modified as follows where we abbreviate the time derivative by $\dot{} = \frac{d}{dt}$:

$$\dot{P}_{126}(t) = (1 - s_C) \sigma_{126 \leftarrow 226} J_X(t) P_{226}(t) - \sigma_{126} J_X(t) P_{126}(t) - \Gamma_{E,126} P_{126}(t) - \Gamma_{R,126} P_{126}(t) \quad (9)$$

$$\begin{aligned} \dot{P}_{125}(t) = & s_C \sigma_{126 \leftarrow 226} J_X(t) P_{226}(t) + \sigma_{125 \leftarrow 225} J_X(t) P_{225}(t) + \sigma_{125 \leftarrow 126} J_X(t) P_{126}(t) - \sigma_{125} J_X(t) P_{125}(t) , \\ & - \Gamma_{E,125} P_{125}(t) + \Gamma_{R,125 \leftarrow 116} P_{116}(t) + \Gamma_{R,125 \leftarrow 026} P_{026}(t) - \Gamma_{R,125} P_{125}(t) . \end{aligned} \quad (10)$$

There is also the possibility that two valence electrons are liberated in the course of K -shell ionization for a high enough x-ray energy. However, the ratio of triple ionization to single ionization is only 0.02 [table III of Ref. 52] which is too small to have a noticeable impact on the ion yields or photon yields in this article. Consequently, this process is neglected in what follows.

Along the lines of the preceding paragraph, photoionization shake off in the course of valence ionization [52] is treated. Namely, multiple photoionization of valence electrons occurs if the x rays have sufficient energy to double-valence-ionize the atom. For x rays above 250 eV the ratio of double to single ionization is saturated and amounts to 16% [table I of Ref. 52]. Likewise to (9), we modify the rate equations for 225 and 216; analogous to (10) the rate equations for 224 [Eq. (11) below] and 215 are changed. Triple and quadruple valence ionization with the saturated ratios of 0.014 and 0.002, respectively, are not included because they are very small.

2. Modified rate equations due to double Auger decay

Double Auger decay [55, 56] occurs for Ne $1s$ holes—where two electrons are emitted instead of one—with a probability of 5.97% of all K -shell holes [table I of Ref. 53]; normal Auger decay takes place for 92.67% of the decays. Triple Auger decay makes only a negligible contribution of 0.38% and is thus not considered here. The remaining probability is due to radiative decay producing Ne^+ ; this is treated already in our plain rate equations (8). Hence, if an electronic decay takes place, double Auger decay occurs with a proba-

bility of $d = \frac{0.0597}{0.0597+0.9267} = 0.06052$ and normal Auger decay with probability $1-d = 0.9395$. Here d includes direct and cascade processes [55]; direct decay refers to the simultaneous emission of two electrons; cascade decay of a Ne $1s$ hole means that there is first normal Auger decay of the vacancy to a short-lived excited state of Ne^{2+} for which the $2s$ subshell is not fully occupied and one electron is in a Rydberg orbital (see Refs. 57–60); then a second electronic decay takes place producing the final state of Ne^{3+} . We do not distinguish these two types of double Auger decay but treat them jointly because the relevant excited states of Ne^{2+} necessary to describe cascade decay are not incorporated in the plain rate equations (8). From the probability of 5.97% for double Auger decay of a K -shell vacancy in Ne one obtains the double Auger partial probabilities for the production of final configurations of Ne^{3+} [column “Total DA” in table I of Ref. 54]; they are $p_{2p^{-3}} = 2.5/100$, $p_{2s^{-1}2p^{-2}} = 2.9/100$, and $p_{2s^{-2}2p^{-1}} = 0.5/100$ for the distribution of the three defect electrons over the valence shell of Ne^{3+} . The total is $p_{\text{DA}} = p_{2p^{-3}} + p_{2s^{-1}2p^{-2}} + p_{2s^{-2}2p^{-1}} = 0.059$. Double Auger decay opens up an additional channel to normal Auger decay. Therefore, we need to introduce an extra electronic decay term in the plain rate equations (8). Yet the emission of the second electron in double Auger decay is triggered by the emission of the first electron [55] and thus not independent of the width for normal Auger decay. We find the fractions $d_{223 \leftarrow 126} = \frac{p_{2p^{-3}}}{p_{\text{DA}}} d$ and, analogously, $d_{214 \leftarrow 126}$ with $p_{2s^{-1}2p^{-2}}$ and $d_{205 \leftarrow 126}$ with $p_{2s^{-2}2p^{-1}}$. They quantify the fraction of $\Gamma_{E,126}$ to end up in the configurations 223, 214, or 205. Furthermore, we let $d_{126} = d_{223 \leftarrow 126} + d_{214 \leftarrow 126} + d_{205 \leftarrow 126}$. To describe double Auger decay, we modify the rate equations via

$$\begin{aligned} \dot{P}_{224}(t) = & (1 - d_{126}) \Gamma_{E,224 \leftarrow 126} P_{126}(t) + \sigma_{224} J_X(t) P_{224}(t) + \sigma_{224 \leftarrow 225} J_X(t) P_{225}(t) \\ & + s_V \sigma_{225 \leftarrow 226} J_X(t) P_{226}(t) + \Gamma_{R,224 \leftarrow 125} P_{125}(t) + \Gamma_{R,224 \leftarrow 215} P_{215}(t) \end{aligned} \quad (11)$$

$$\begin{aligned} \dot{P}_{223}(t) = & d_{223 \leftarrow 126} \Gamma_{E,126} P_{126}(t) + \sigma_{223 \leftarrow 224} J_X(t) P_{224}(t) - \sigma_{223} J_X(t) P_{223}(t) + \Gamma_{E,223 \leftarrow 125} P_{125}(t) \\ & + \Gamma_{R,223 \leftarrow 214} P_{214}(t) + \Gamma_{R,223 \leftarrow 124} P_{124}(t) . \end{aligned} \quad (12)$$

Likewise to Eq. (11), the rate equations for 215 and 206 are changed, the one for 206, however, without valence shake off term “ s_V ”. Analogous to Eq. (12), we modify the rate equations for 214 and 205.

IV. PATH ANALYSIS

A. Weights and probabilities of paths

The plain rate equations (8) tell us how probability flows through the graph [51] in figure 2. However, from

the solution of (8), we cannot easily identify what pre-dominant mechanisms are at work in the interaction with the x rays. In Ref. 12, stepwise absorption of x-ray photons by core electrons “C” [61] with subsequent Auger decay “A” is proposed as prevailing mechanism, if energetically allowed. Otherwise only valence ionization “V” occurs. This inference is based on the Auger electron yield [32]. In what follows, we analyze in detail this proposition and, thereby, devise an analysis to elucidate the processes responsible for reaching a configuration and the probability for doing so.

Figure 2 shows a simple and directed graph [51]. Simple graph means that multiple edges and loops are disallowed and directed graph indicates that the edges have orientations. If the x-ray energy is high enough such that all configurations in figure 2 can be reached, it is a connected graph, i.e., it contains one directed path between every pair of vertices; otherwise it is a disconnected graph as certain configurations cannot be populated. The vertices are the cationic configurations of the atom (1). They are arranged from top to bottom in rows where each row corresponds to a specific charge state of the atom. Within a row the configurations are sorted from left to right with increasing energy. The edges in the graph are the transitions. With the concept terminal configuration we denote configurations that are not subject to electronic or radiative decay. The atom remains in such a configuration unless photoionization takes place. In the graph in figure 2, the terminal configurations are at the very left, i.e., they are the energetically lowest configuration in each charge state. Thus there is one terminal configuration per charge state.

Looking at figure 2, we face a complicated situation; typically, there are many paths that start at the neutral atom and lead to the same last configuration. We need to identify those ones which are really important, i.e., dominant paths. To do so, first, all possible paths are required and, second, these paths need to be assigned probabilities to assess their contribution to reach a specific configuration. All possible paths are generated with a recursive algorithm [62]. The length of a path is the number of configurations it traverses. The path of length one is the path that starts and also ends in the configuration of the neutral atom. The paths of length two start from the neutral atom and consider an additional photoionization [figure 2]. The paths of length three add either another photoionization or a decay process to the paths of length two. This algorithm continues to generate paths of increasing length until the electron-bare configuration of the atom is reached. To limit the total number of paths, we only consider radiative decay in paths, if no competing Auger decay is present. As radiative decay is so much slower than Auger decay, figure 1, the omitted paths do not carry a noticeable probability for the analysis to follow.

So far we know only all possible paths in the graph [51] in figure 2 connecting the neutral atom with any other configuration. Yet there is a difference between the im-

portance of a photoionization, Auger decay, or radiative decay to occur, i.e., a specific probability is associated with each process depending also on the configuration from which they originate and its population during the interaction with the x rays. Depending on the number and kind of transitions in a path, it has a certain weight for reaching a specific configuration. To find these weights, we start by obtaining the probabilities of an atom in configuration $i \in \mathbb{K} \wedge i \neq 000$ to undergo photoionization or decay in figure 2 from the probabilities $P_i(t)$ of (8). This corresponds to taking the terms on the right-hand side of (8) which cause a reduction of the rate, i.e., those with a minus sign. To determine the probability for photoionization, we integrate

$$\frac{d}{dt} Q_{P,i}(t) = \sigma_i P_i(t) J_X(t), \quad (13)$$

and for decay processes, we integrate

$$\frac{d}{dt} Q_{k,i}(t) = \Gamma_{k,i} P_i(t), \quad (14)$$

with $k \in \{E, R\}$ where E denotes electronic decay and R stands for radiative decay. Initially, we have $\lim_{t \rightarrow -\infty} Q_{k,i}(t) = 0$ with $k \in \{P, E, R\}$. From the probabilities $Q_{k,i}(t)$, we determine branching ratios

$$B_{k,i} = \lim_{t \rightarrow \infty} \frac{Q_{k,i}(t)}{Q_{P,i}(t) + Q_{E,i}(t) + Q_{R,i}(t)}, \quad (15)$$

which give the fraction of atoms in the configuration i that undergo a process $k \in \{P, E, R\}$.

Equipped with the paths and the branching ratios, we can assign weights to the paths. The path of length one, the neutral atom, has unit weight. To find the weight of a path with a certain length greater than one, we multiply the weight of the path of length minus one by the fraction $\frac{\sigma_{j \leftarrow i}}{\sigma_i} B_{P,i}$ for a photoionization and by $\frac{\Gamma_{k,j \leftarrow i}}{\Gamma_{k,i}} B_{k,i}$ for a decay with $k \in \{E, R\}$ where the last configuration of the path with length minus one is i and the last configuration of the path with length is j . Sums of the path weights for all configurations of a fixed charge state—along horizontal lines in the graph [51] in figure 2—give unity provided that no paths are omitted and double counting is removed: the first condition refers to our recursive algorithm [62] which omits radiative transitions if a competing Auger decay is present; the second condition implies that paths with trailing radiative transitions are disregarded in the sum over the weights. The fact that the sum of the path weights under the previous conditions is unity is because starting from the neutral atom with unit probability, the paths leading to configurations of a chosen charge state reveal how this unit probability diffuses over these configurations. But the paths leading to non-terminal configurations have no relevance for our analysis because no probability remains in those configurations for $t \rightarrow \infty$ as they are connected by radiative transitions to terminal configurations. Hence these paths can be suppressed altogether.

TABLE I. Paths with maximum probability for the terminal configurations of neon. Here “Config.” is the cationic configuration, “Paths” is the number of paths leading to the configuration, “Unique” is the number of paths with unique strings, “Norm.” is the number of paths with unique normalized strings, “String” is the string of the path with maximum probability “Probability”, and “Term. prob.” is the terminal probability in the configuration. The empty string is ϵ [63]. The photon energy is 1200 eV, the fluence is $8 \times 10^{11} \frac{\text{photons}}{\mu\text{m}^2}$, and the pulse duration (FWHM) is 100 fs. Number of paths counts also paths which have zero weight because of the photon energy being too low for the involved photoionization channels.

Config.	Paths	Unique	Norm.	String	Probability	Term. prob.
226	1	1	1	ϵ	2.8×10^{-7}	2.8×10^{-7}
225	2	2	2	V	9.5×10^{-7}	9.5×10^{-7}
224	9	8	6	CA	4.2×10^{-5}	4.2×10^{-5}
223	45	30	8	VCA	3.8×10^{-5}	7.7×10^{-5}
222	237	115	18	CACA	5.8×10^{-4}	6.2×10^{-4}
221	1261	441	22	VCACA	2.3×10^{-4}	8.0×10^{-4}
220	6719	1693	41	CACACA	2.8×10^{-3}	3.5×10^{-3}
210	27403	4128	41	VCACACA	1.2×10^{-3}	7.9×10^{-3}
200	185016	19067	119	CACACACA	2.0×10^{-2}	3.1×10^{-1}
100	574522	58364	175	CACACACAC	4.3×10^{-2}	6.8×10^{-1}
000	806829	81803	175	VCACACDVVV	2.2×10^{-7}	3.1×10^{-6}

To convert the weights of the paths into probabilities, we divide the weight of a path ending in a terminal configuration by the sum of all the weights of the paths that lead to this terminal configuration multiplied by the terminal probability of that configuration. Paths that lead to non-terminal configurations consequently have zero probability. This assigns a probability to each path that indicates its contribution to the probability found in the configuration at its last vertex for $t \rightarrow \infty$.

B. Formal language and summed quantities

With the probabilities of the paths from the previous section IV A, we can now figure out which paths are most important to reach a chosen configuration. For neon, we have a total number of paths of 2 051 874 and 1 602 044 many paths lead to its terminal configurations. In order to symbolize paths, we introduced the alphabet [63] “ACV” at the beginning of section IV A. Thereby, we disregard a distinction of ionization from $2s$ or $2p$ subshells of neon and summarize such an ionization under the letter “V”. We would like to extend the alphabet to include photoionization of the remaining core electron of a single core hole producing a double core hole “D” and radiative decay “R”. With this alphabet “ACDRV”, we can form strings (or words) [64] that represent the transitions in a path. A path of a certain length has length minus one transitions, i.e., it is described by a string of length minus one. The path starting and ending in the neutral atom is represented by the empty string ϵ [63]. This identification allows us to understand the algorithm [62] to generate the paths in the graph of figure 2 as a formal grammar [65] that specifies the words [64], i.e., the strings, over the given

alphabet [63] of the formal language [66]. This approach already reduces the intricacy of the problem. We still have many paths which does not reveal interesting information.

First, we determine the path with maximum probability for each terminal configuration in table I. As we thus select only a single path per charge state, the associated values in the column “Probabilities” in table I do not sum to unity. However, because the atom is in some terminal configuration after the interaction, the values in the column “Term. prob.” do sum to unity. We find that, indeed, for the specified pulse parameters “CA” processes dominate as proposed in Refs. 12 and 32. Valence ionization is only present, if the terminal configuration cannot be reached by “CA” processes, i.e., an odd number of electrons is missing or the x-ray energy is too low for “C” to occur. Comparing the probabilities of the paths with maximum probability with the terminal probabilities reveals that even for the configuration 225 there is no agreement and the former is lower than the latter when more digits are considered than shown in table I. Namely, as the sum of the probabilities of all paths that lead to a terminal configuration is the terminal probability, there needs to be an additional path that accounts for the discrepancy. In this case, it is “VR”, i.e., valence ionization of 226 to 216 with ensuing radiative decay to 225. Yet for higher charged configurations, it turns out that the path with maximum probability contributes only a small amount to the terminal probability trapped in a configuration [table I].

Second, for configurations 224, \dots , 000 multiple paths with the same string arise that contribute comparatively to the terminal probability. This is due to the reduced level of detail by introducing letters for processes which summarize different configurations under a single letter. As there is no distinction made between paths

TABLE II. Paths with a probability greater than 10^{-5} for selected terminal configurations of neon. Here “Probability” is the sum of the probabilities of all paths with the same “String” and “Sum” is the sum of the probabilities of the paths shown for a configuration in the table. Other parameters as in table I.

Config.	String	Probability	Sum
223	VCA	3.8×10^{-5}	7.7×10^{-5}
	CAV	3.4×10^{-5}	
222	CACA	5.8×10^{-4}	6.2×10^{-4}
	CDAA	3.2×10^{-5}	
221	VCACA	2.3×10^{-4}	7.7×10^{-4}
	CAVCA	2.1×10^{-4}	
	CACAV	1.8×10^{-4}	
	CACVA	5.0×10^{-5}	
	CVACA	3.3×10^{-5}	
	VCDAA	2.1×10^{-5}	
	VCACAR	1.9×10^{-5}	
	CAVCAR	1.7×10^{-5}	
	CACAVR	1.3×10^{-5}	

with the same strings, we sum over their probabilities and thus remove these duplicates. This significantly reduces the number of paths to be considered [table I]. Taking into account the paths with highest probability, table II, provides an understanding of the terminal configurations 223, 222, and 221. For 223 there are two dominant paths, “VCA” and “CAV”, which make up most of the probability. The “CAV” has a slightly lower probability than “VCA” because there are fewer valence electrons available for the “V” transition. The string “CVA” has a much smaller probability as, in this case, the short core-hole lifetime sets a time scale during which a valence electron needs to be ionized. For 222 and 221 we find a small admixture of paths with double core holes. Finally, for 221 several paths contribute comparatively which are distinguished by the position of the “V”. For higher charge states, too many paths make a noticeable contribution to the terminal probability for an analysis using the strings so far introduced to be conclusive [42].

Third, for the highest-charged configurations 210, ..., 000, there are so many different paths to reach them that it is hard to extract a few which are dominant. Hence, we take another step to simplify the problem and introduce normalized strings. These are the previously introduced strings whose characters we sort in the order they appear in the latin alphabet. Then we may sum the probabilities for the same normalized strings which greatly reduces the number of strings to consider [table I]. This facilitates to extract a few important ionization pathways listed in table III. Even for the highest charge states, the number of normalized strings of relevance remains manageable. We note an increasing relevance of paths with double core holes for

TABLE III. Normalized path strings with a probability in the highest two orders of magnitude for the probability of selected terminal configurations of neon. Here “Norm. string” is a normalized string and “Probability” is the sum over the probabilities of all paths with the same normalized string. Other labels and parameters as in table I and II.

Config.	Norm. string	Probability	Sum
221	AACCV	7.0×10^{-4}	8.0×10^{-4}
	AACCRV	5.7×10^{-5}	
	AACDV	3.8×10^{-5}	
220	AAACCC	2.8×10^{-3}	3.4×10^{-3}
	AAACCD	4.0×10^{-4}	
	AAACCCR	2.6×10^{-4}	
210	AAACCCV	6.0×10^{-3}	7.7×10^{-3}
	AAACCDV	1.1×10^{-3}	
	AAACCCRV	6.1×10^{-4}	
200	AAAACCCC	1.6×10^{-1}	2.9×10^{-1}
	AAAACCCD	5.5×10^{-2}	
	AAACCCRV	5.1×10^{-2}	
100	AAACCCDRV	1.9×10^{-2}	6.6×10^{-1}
	AAAACCCCC	3.5×10^{-1}	
	AAAACCCCD	1.2×10^{-1}	
	AAACCCCCRV	1.1×10^{-1}	
	AAACCCCDRV	4.1×10^{-2}	
	AAACCCCVV	2.5×10^{-2}	
	AAAACCCDD	1.1×10^{-2}	
	AACCCDVVVV	2.5×10^{-6}	
000	AACCCDVVVV	2.5×10^{-6}	3.0×10^{-6}
	AACCCDDVVVV	4.7×10^{-7}	

higher charge states.

Forth, the most drastic simplification of the problem is to disregard the types of transitions occurring and to consider only the length of the paths leading to a terminal configuration and sum over all path probabilities with this length. From table IV, we realize that this simplification leads to only one, two, or three path lengths that make a substantial contribution to the probability of a terminal configuration. The minimum path length to reach a specific charge state is, thereby, given by the number of electrons that need to be removed. It turns out, table IV, that this already leads to the paths which make the most important contribution. Electrons are removed by “A”, “C”, “D”, “V” transitions whereas “R” transitions leave the electron number unchanged. Thus paths longer than the minimum length contain “R” transitions which are slow compared with “A” transitions and, at high x-ray intensity, with “C”, “D”, “V” transitions [figure 1]. The maximum path length specified in table IV is somewhat shorter than it could be because we neglected radiative transitions if a competing Auger decay is present.

TABLE IV. Length of path strings with a summed probability in the highest three orders of magnitude of the probability for the terminal configurations of neon. Here “Min.” refers to the minimum path length possible, “Max.” to the maximum path length, and “Len.” to the path length associated with “Probability”. Other labels and parameters as in table I and II.

Config.	Min.	Max.	Len.	Probability	Sum
226	0	0	0	2.8×10^{-7}	2.8×10^{-7}
225	1	2	1	9.5×10^{-7}	9.6×10^{-7}
			2	1.2×10^{-9}	
224	2	4	2	4.2×10^{-5}	4.2×10^{-5}
223	3	6	3	7.7×10^{-5}	7.7×10^{-5}
			4	3.4×10^{-7}	
222	4	8	4	6.2×10^{-4}	6.2×10^{-4}
			5	1.6×10^{-6}	
221	5	10	5	7.4×10^{-4}	8.0×10^{-4}
			6	6.0×10^{-5}	
220	6	12	6	3.2×10^{-3}	3.5×10^{-3}
			7	3.1×10^{-4}	
210	7	13	7	7.2×10^{-3}	7.9×10^{-3}
			8	7.2×10^{-4}	
200	8	15	8	2.3×10^{-1}	3.1×10^{-1}
			9	7.6×10^{-2}	
			10	1.4×10^{-3}	
100	9	16	9	5.1×10^{-1}	6.8×10^{-1}
			10	1.6×10^{-1}	
			11	3.0×10^{-3}	
000	10	17	10	3.0×10^{-6}	3.1×10^{-6}
			11	3.2×10^{-8}	

V. ION YIELDS OF NEON ATOMS

Rate equations [section III] provide time-dependent probabilities to find an atom in a configuration. Such a time-dependent population is difficult to measure. Therefore, ion yields are considered instead which are derived from the probability at infinite time to find the atom in a specific charge state renormalized to the probability to find an ion then at all [13, 15]. Ion yields are experimentally accessible via the ion time-of-flight [9, 12]. Furthermore, they have the decisive advantage that, unlike probabilities, they do not depend on the geometry of the interaction volume or the gas density. In what follows, we compare theoretical ion yields from our rate equations [section III] with previously obtained theoretical and experimental data for neon in LCLS radiation [12, 17].

In figure 3, we show the ion yields of neon for the x-ray energies of 1110 eV (upper panel) and 1225 eV (lower panel). There is almost no yield for Ne^{10+} as the photon energy is, in both cases, below the core-ionization threshold of Ne^{9+} . We compare the theoretical ion yields

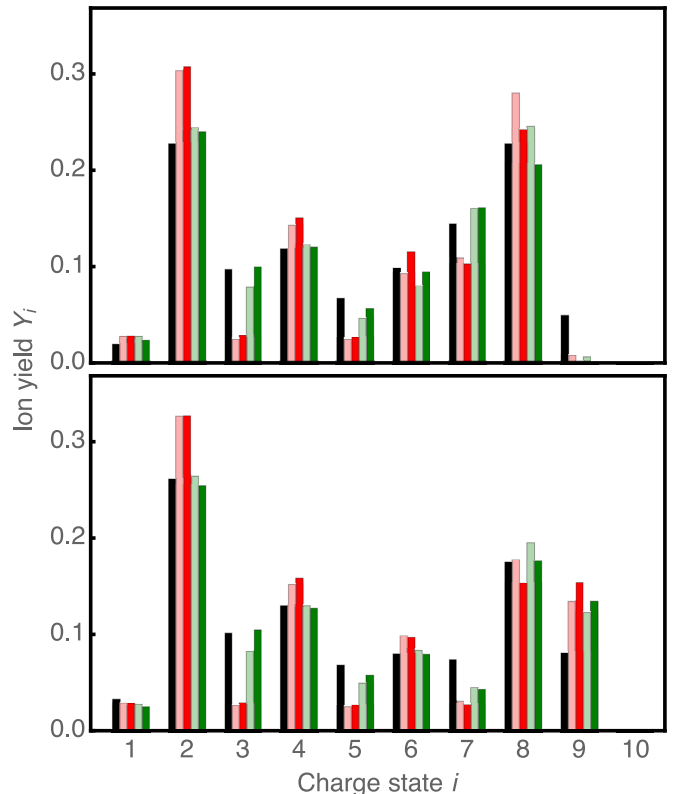


FIG. 3. (Color online) Ion yields of neon atoms in LCLS radiation at photon energies of 1110 eV (upper panel) and of 1225 eV (lower panel). **Black** bars represent experimental data from figure 2 in Ref. 17 for a FWHM pulse duration of 100 fs. The nominal pulse energies are 1.27 mJ (upper panel) and 1.45 mJ (lower panel). In both cases, we assume a reduction of the nominal pulse energy by a factor of 0.699/3 due to transmission losses in the x-ray optics. This factor is not specified in Ref. 17 but is taken from Ref. 12 for a photon energy of 1050 eV. The Gaussian beam is taken to have a FWHM major axis of $2 \mu\text{m}$ and a FWHM minor axes of $1 \mu\text{m}$ as in Ref. 12; in Ref. 17 only an approximate beam area of $\sim 2 \mu\text{m}^2$ is noted. **Light red** and **light green** bars are the theoretical ion yields from figure 2 in Ref. 17 without and with inclusion of shake off, respectively. **Red** bars show our predictions with the plain rate equations [section III A] and **green** bars stand for the ion yields from the modified rate equations [section III B].

from our plain rate equations [section III A] to the equivalent in Ref. 17 which were obtained with the rate equations from Ref. 32 and find the results of both computations to be very similar. There is a pronounced asymmetry between even and odd charge states in the theoretical values apart from Ne^{9+} in the lower panel. Namely, the ion yields for odd charge states are generally much lower than for even charge states. This is because the dominant paths in the plain rate equations are mainly composed of sequences of “CA” processes [table I] which cause an even number of electrons to be removed from the atom and are the principal contribution to produce even charge states. For the odd charges states, mostly an ad-

ditional valence ionization needs to occur, i.e., the string starts with “V” [table I], which suppresses such paths. However, this asymmetry between odd and even charge states in the theoretical ion yields is not as pronouncedly reflected in the experimental ones; apart from Ne^+ , for the odd charges states, we find that the measured ion yields are drastically underestimated by the plain rate equations apart from Ne^{9+} in the lower panel. This poor agreement of theory with experiment has already been noted in Ref. 12. It hints at the omission of further ionization channels that cause an increase of the odd charge states.

The ion yields from the modified rate equations [section IIIB] are also presented in figure 3. We observe a large improvement over the ion yields from the plain rate equations [section IIIA] leading to a good agreement with the experimental data for most charge states. Specifically, the theoretical ion yields from our modified rate equations are very similar to those obtained with the theory of Ref. 17 that includes theoretical calculations of single and double shake off after K -shell ionization. This mitigates the previously found asymmetry between odd and even charge states because single photoionization shake off for Ne—the only one considered by us in section IIIB—removes an additional electron over the primary ionization. Thereby, shake off increases the ion yield of Ne^{2+} and, if a K -shell hole is created, makes upon Auger decay a (transient) contribution to Ne^{3+} . Likewise, double Auger decay of a K -shell vacancy in Ne^+ makes a (transient) contribution to Ne^{3+} . However, the agreement between theory and experiment is not always good, namely, for the ion yields of Ne^{7+} (lower panel) and Ne^{9+} (both panels). The Ne^{9+} ion yield in the upper panel is far too low because simultaneous two-photon ionization [17] is not included in our modified rate equations. The discrepancy in the Ne^{7+} ion yield in the lower panel can be ascribed to an inner-shell resonant excitation [17] which is not included in our modified rate equations. Such resonant processes have a significant impact on the ion yields for an x-ray energy of 1050 eV [34] (see below).

In figure 4, we display the ion yields of neon for the x-ray energies of 800 eV (upper panel), 1050 eV (middle panel), and 2000 eV (lower panel). In the upper panel, ion yields from the theory of Ref. 32 are compared with results from our plain rate equations [section IIIA] and very good agreement between both and the experimental data is observed [67]. Here the x-ray energy is below the K -shell ionization threshold where photoionization shake off with respect to core ionization and double Auger decay do not occur. Yet there is still photoionization shake off from valence ionization, an effect that has hitherto been disregarded. Our modified rate equations [section IIIB] showcase the importance of this effect which lifts the good agreement between theory and experiment. In the middle and lower panels, we have a situation very much like the one in figure 3 and large parts of its discussion is relevant here as well. As before,

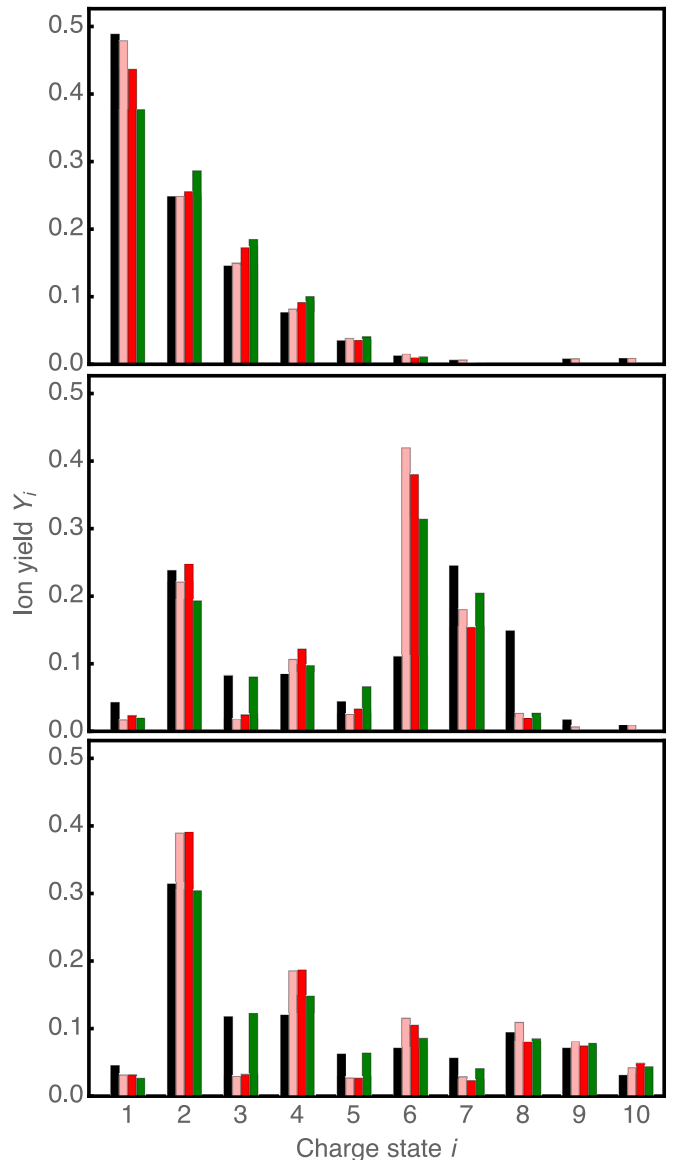


FIG. 4. (Color online) Ion yields of neon atoms in LCLS radiation at photon energies of 800 eV (upper panel), of 1050 eV (middle panel), and of 2000 eV (lower panel). Experimental data stems from Fig. 2b in Ref. 12. From top panel to bottom panel, the FWHM pulse durations are 340 fs, 280 fs, and 230 fs, respectively; the nominal pulse energy is 2.4 mJ which needs to be multiplied by the factors 0.663/3, 0.699/3, and 0.584/3, respectively, to obtain the actual pulse energies. Our prediction for 2000 eV photon energy is made using a factor of 0.25 instead of $0.584/3 = 0.195$ and a FWHM x-ray beam diameter of $1 \mu\text{m}$. See text for further details. Everything else as in figure 3.

the plain rate equations give rise to ion yields which are in stark discrepancy from the ones found in the experiment. The inclusion of photoionization shake off and double Auger decay in the modified rate equations leads to an overall satisfactory agreement between theory and experiment. However, specifically in the middle panel,

there is a drastic discrepancy discovered for Ne^{6+} and Ne^{8+} . In Ref. 34, this case is investigated and the observed deviations are ascribed to resonant excitations which are not included in our modified rate equations. For the lower panel, we use different parameters than those in Ref. 12. Otherwise no agreement—not even with the published theoretical ion yields and our plain rate equations—is obtained. Our choice of parameters produces a peak intensity of $2.2 \times 10^{17} \frac{\text{W}}{\text{cm}^2}$ which is consistent with $4.5 \times 10^{17} \frac{\text{W}}{\text{cm}^2}$ at a FWHM pulse duration of 140 fs used in Ref. 35 to produce similar theoretical ion yields as the ones shown in the lower panel with the modified rate equations. To achieve about the intensity of Ref. 35 we reduced the FWHM spot size of the x-ray beam. Without reducing the spot size, we would need a factor of 0.635 instead of 0.25 to determine the actual pulse energy from the nominal one; we consider this to be unrealistically high. Certainly, reducing the spot size of the x-ray beam significantly is questionable as well because the design limit of the x-ray optics is specified in Ref. 12 to be just our value of a FWHM beam diameter of 1 μm .

Overall, we note that there is a good agreement between the theory of this work and the one of Refs. 12 and 17. The observed variations do not originate from differences in the Auger decay widths between ours and the ones from Ref. 38—on which the theoretical computations of Refs. 12 and 17 are based—turn out to have a small influence [42]. This can be ascribed to the dominance of “CA” style paths [table I] instead of double core holes in the interaction with the x rays because a precise timing of the Auger decay is not important then. We use the nominal pulse duration in all calculations. However, the actual pulse duration was measured to be much shorter in experiments [12, 68]. As noticed in [13], there is only a small influence on the ion yields, if, e.g., the pulse duration is halved, again, because of the prevalence of “CA” style paths. There still remains uncertainty about the actually available pulse energy for the experimental data of Ref. 12 and 17. In Ref. 33 the authors report that the pulse energy needed to be increased compared with the values of Ref. 12 to reproduce the theoretical ion yields there. In principle, we expect that the actual pulse energy at the sample should be obtainable by comparing the experimental Ne^+ ion yield computed considering only the amount of Ne^+ and Ne^{2+} ionization with the theoretical one from the modified rate equations [section III B] which include all relevant physical effects. Yet this approach does not work in practice [42] seemingly as the experimental parameters, such as the spot size of the beam, are insufficiently well known. In Ref. 35, the consequences of direct double Auger decay of a K -shell vacancy in Ne^+ is examined for the prediction of the ion yields in the lower panel of figure 4; there, it is claimed that shake off due to Auger decay was treated in [17]. Yet knock off is found to be the more important contribution [35]. The impact of double Auger decay of a $\text{Ne} 1s$ hole is also found to be significant by us [42]—it

chiefly influences the ion yields of Ne^{2+} and higher odd charge states—just as the impact found for direct double Auger decay studied in Ref. 35.

VI. PHOTON YIELDS OF NEON ATOMS

Studying the fluorescence of multiply-charged atoms allows one deep insights into the involved states in the radiative transitions. This provides much more detailed information compared with ion yields [section V]. Fluorescence spectroscopy complements Auger electron spectroscopy [21, 56]. The latter has been used so far in LCLS experiments [10, 11]. A drawback of fluorescence spectroscopy is the low fluorescence yield for light elements [section II B].

To predict fluorescence spectra based on rate equations, we calculate the probability for photon emission $F_{j \leftarrow i}(t)$ up to time t for the transition $i \rightarrow j$ with $i, j \in \mathbb{K}$ [Eq. (1)], via

$$\frac{d}{dt} F_{j \leftarrow i}(t) = \Gamma_{R, j \leftarrow i} P_i(t). \quad (16)$$

Initially, we have $\lim_{t \rightarrow -\infty} F_{j \leftarrow i}(t) = 0$. Equation (16) is analogous to Eq. (14) for $k = R$ and, in fact, $F_{j \leftarrow i}(t) = \frac{\Gamma_{R, j \leftarrow i}}{\Gamma_{R, i}} Q_{k, i}(t)$ holds, if i is not a terminal configuration, i.e., $\Gamma_{R, i} \neq 0$. The probability for photon emission is experimentally only very difficult to access because it depends on the precise geometry of the interaction volume and the gas density within it. Theoretically, this implies that the probability depends on the size of the beam cross section we integrate over.

From the probability for fluorescence photon emission, we calculate the easily experimentally accessible photon yield $y_{j \leftarrow i}$ for the radiative transition $i \rightarrow j$ which is independent of the detailed characteristics of the interaction volume just like the ion yields from section V; it is defined by

$$y_{j \leftarrow i} = \lim_{t \rightarrow \infty} \frac{F_{j \leftarrow i}(t)}{\sum_{k, l \in \mathbb{K}} F_{l \leftarrow k}(t)}, \quad (17)$$

for $i, j \in \mathbb{K}$. In the denominator, we sum over all radiative transitions, i.e., we calculate the total probability for fluorescence photon emission. The photon yield is expressed as a spectrum via

$$y(\omega) = \sum_{j, i \in \mathbb{K}} y_{j \leftarrow i} \delta_{\omega E_{R, j \leftarrow i}}, \quad (18)$$

and the Kronecker- δ [69]. Here $E_{R, j \leftarrow i}$ is the radiative transition energy analogous to Eq. (3).

The photon yields of neon are displayed in figure 5. Several strong XUV and x-ray lines are discernible. Those radiative transition which have no competing Auger decay exhibit the strongest photon yield, e.g., the strongest

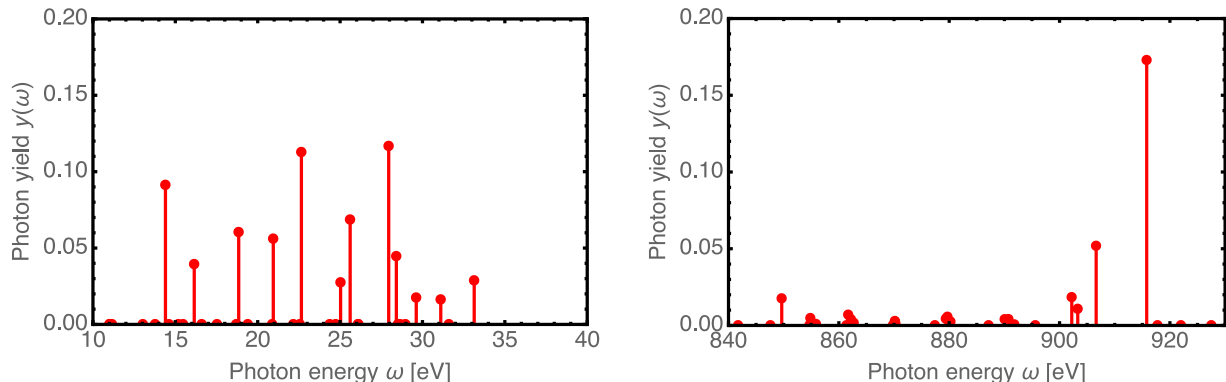


FIG. 5. (Color online) Photon yields (18) of neon in the XUV (left) and the x-ray (right) regime. The pulse energy is 2.4 mJ, the photon energy 1200 eV, pulse duration (FWHM) is 100 fs, and 25% transmission of the nominal x-ray pulse energy. The Gaussian beam has a FWHM major axis of $2\ \mu\text{m}$ and a FWHM minor axes of $1\ \mu\text{m}$.

x-ray line at 915.80 eV stems from the radiative transition $101 \rightarrow 200$. Particularly, all XUV lines originate from the exclusively radiative decay of configurations with fully occupied $1s$ shell, e.g., the strongest XUV line at 27.95 eV is from $215 \rightarrow 224$. As the x-ray pulse is spatially a Gaussian beam, there are large areas of its cross section where the associated x-ray flux is comparatively low such that, at most, one x-ray is absorbed which produces predominantly a single core hole. Hence the fairly strong fluorescence on the $126 \rightarrow 225$ transition at 849.65 eV despite the competing Auger decay. Recording the XUV lines in an experiment reveals rich information about the interaction of the atom with x-rays because it indicates the population of a specific configuration which is produced by the x-ray pulse as radiative decay is so slow that hardly any takes place during an ultrashort x-ray pulse. This allows one insights into the kind of x-ray processes that have occurred. Another advantage of also recording the XUV spectrum is that one has simply more lines to measure compared with the x-ray spectrum as there are 12 radiatively-decaying configurations without competing Auger decay in the former case compared with 4 in the latter one [see Eq. (19) below]. However, figure 5 reveals that despite competing Auger decay, more x-ray lines, nonetheless, are relevant than predicted by this simple argument. We observe that inaccuracies in the Auger decay widths have only a small effect on photon yields [42].

VII. COMPUTATIONAL DETAILS

A. Complete atomic electronic structure for rate equations

To carry out the atomic electronic structure computations from section II, we developed the program CAESR (Complete Atomic Electronic Structure for Rate equations) as part of the FELLA package [70]. This program generates all configurations and invokes GRASP2K [46,

47] and RATIP [48] with the appropriate input files. Afterwards CAESR analyses the output and processes the results.

We use the version 1 programs of the year 2013 edition of GRASP2K [46, 47]. In the computations, we use an atomic mass number of 20 for neon and a mass of the nucleus of 20.1797 u [71]. Thereby, we assume the most abundant isotope of neon which has a vanishing nuclear spin, nuclear dipole moment, and nuclear quadrupole moment [72]. For less than 50 energy levels (always the case for neon), CAESR performs an extended-optimal-level (EOL) computation [45] which, however, becomes unreliable due to singular energy levels beyond this threshold. Above 50 levels, CAESR switches to an extended-average-level (EAL) computation [45]. EOL is more suited for some cases with few electrons for which EAL does not converge. We require a minimum amount of orbital convergence of 10^{-5} in MCDHF computations.

For the RATIP [48] programs, CAESR initially determines the states of the multiplet for each cationic configuration of an atom apart from the electron-bare nucleus. This is accomplished by representing the Hamiltonian in the basis of the configuration state functions of the multiplet and diagonalizing it fully with RELCI [48, 73]. The Hamiltonian, thereby, comprises the contributions of the frequency-independent Breit interaction, the vacuum polarization, and the specific mass shift. REOS is used to determine radiative transitions in the Babushkin gauge. It relies on a complete expansion of the atomic state functions in a determinant basis with CESD. No orthogonality is assumed in REOS between the orbital sets of the initial and final atomic states. For neon the lowest multipole order of the radiative transition is E_1 on configuration level, if an electron falls down from a p subshell to an s subshell and M_1 and E_2 for transitions involving the multiplets of configurations differing by two s subshells. For atoms with a higher atomic number than neon, more cases arise. If M_1 and E_2 are the lowest order multipoles, we determine both radiative decay widths and add them. AUGER and PHOTO are employed to calculate the elec-

tronic decay widths and photoionization cross sections, respectively. In both cases orthogonality between the sets of orbitals of the initial and final atomic states is assumed. Also a continuum electron is emitted for both quantities; its wave function is determined including exchange interactions with the parent ion for AUGER and without it for PHOTO. The photoionization cross sections are computed in Babushkin gauge in E_1 multipole order on a linear-logarithmic grid of energies starting at the ionization threshold of the atom; the first 10 energies are linearly spaced with a step size of 1 eV; the remaining 20 energies are spaced evenly on a decadic-logarithmic grid starting 1 eV above the last energy of the linear grid and ending at 2000 eV. This choice is motivated by the observation that cross sections vary most close to the ionization threshold and very little afterwards.

B. Numerical solution of the rate equations

The x-ray pulse is represented temporally by a Gaussian function [Eq. (7) in Ref. 13]; there is no need to account for the spikiness of SASE pulses from LCLS [13, 32]. Spatially, x-ray pulses are described as a Gaussian beam [Eq. (8) in Ref. 13] with a cross section that has a specific FWHM major and minor axes; longitudinally, the beam has a long Rayleigh length and thus a small variation over the interaction volume, i.e., a longitudinal variation can be neglected [13].

We numerically solve the rate equations [section III] in the time interval $[-10 \text{ ps}; 10 \text{ ps}]$ which is long enough for the x-ray pulse to be over and all Auger decay processes to have taken place. However, we would have to solve the rate equations for an excessively long time interval for radiative transitions to take place where no competing Auger decay is available because the lifetime of radiative decay is so much longer than the one of Auger decay [figure 1]. This is particularly the case for dipole-forbidden transitions. The slowest radiative decay is $110 \rightarrow 200$ with a lifetime of $134 \mu\text{s}$ and the slowest Auger decay is $111 \rightarrow 200$ with a lifetime of 41.7 fs. The relevant radiative transitions are the ones originating from the configurations [Eq. (1)]:

$$\mathbb{D} = \{216, 215, 206, 214, 205, 213, 204, 212, \\ 203, 211, 202, 201, 110, 101, 010, 001\} \subset \mathbb{K}. \quad (19)$$

After the x-ray pulse is over, only decay processes continue to occur. Hence we proceed analogously to Theorem 2 in Ref. 16, i.e., we decompose the solution of the rate equations into a numerical solution up to time \mathfrak{T} and a subsequent evolution in terms of the decay equation [16], i.e., Eq. (8) without terms involving cross sections,

$$\frac{d\mathbf{p}(t)}{dt} = \mathbf{\Gamma} \mathbf{p}(t), \quad (20)$$

yielding $\mathbf{p}(t) = e^{\mathbf{\Gamma}(t-\mathfrak{T})} \mathbf{p}(\mathfrak{T})$. Here the $|\mathbb{K}|$ -many probabilities are aggregated in $\mathbf{p}(t)$ where the initial value $\mathbf{p}(\mathfrak{T})$

is given by the probabilities from the numerical solution at time \mathfrak{T} . In our case, $\mathbf{\Gamma}$ comprises only the radiative decay widths originating from the configurations (19).

If we were only interested in the terminal probabilities, then we would not need to solve (20). Instead, we only needed to sum over the probabilities of each charge state at time \mathfrak{T} ; the sums are then the terminal probabilities. This is what comes out, if the limit $t \rightarrow \infty$ is taken in (21) below ($\mu_\ell \leq 0$). However, numerically integrating (14) ($k = R$) and (16) does require the solution of the rate equations for an excessively long time interval. To accomplish this, we notice that $\mathbf{\Gamma}$ is diagonalizable, and go to its eigenbasis [16] which is a representation of the solution of Eq. (20) for the probability $\mathbf{p}_i(t)$ with $i \in \mathbb{K}$ that is more suited for our purposes

$$\mathbf{p}_i(t) = \sum_{\ell, j \in \mathbb{K}} \mathfrak{U}_{i\ell} e^{\mu_\ell(t-\mathfrak{T})} (\mathfrak{U}^{-1})_{\ell j} \mathbf{p}_j(\mathfrak{T}). \quad (21)$$

Here μ_ℓ and \mathfrak{U} denote the eigenvalue for $\ell \in \mathbb{K}$ and the matrix of eigenvectors of $\mathbf{\Gamma}$, respectively. To numerically integrate (14) ($k = R$) and (16), we need to compute $\int_{\tau}^{\mathfrak{T}} P_i(t') dt' + \int_{\mathfrak{T}}^t \mathbf{p}_i(t') dt'$ where $\tau = -10 \text{ ps}$ here and $t \geq \mathfrak{T} = 10 \text{ ps}$. The second integral is solved with (21) using

$$\int_{\mathfrak{T}}^t e^{\mu_\ell(t'-\mathfrak{T})} dt' = \begin{cases} \frac{e^{\mu_\ell(t-\mathfrak{T})} - 1}{\mu_\ell} & \mu_\ell \neq 0 \\ t - \mathfrak{T} & \mu_\ell = 0 \end{cases} \quad (22)$$

By replacing $e^{\mu_\ell(t-\mathfrak{T})}$ in (21) with (22), we obtain $\int_{\mathfrak{T}}^t \mathbf{p}_i(t') dt'$. We arrive at the probability for photon emission

$$\lim_{t \rightarrow \infty} F_{j \leftarrow i}(t) = F'_{j \leftarrow i}(\mathfrak{T}) + \lim_{t \rightarrow \infty} \left(\mathbf{1}_{\mathbb{D}}(i) \Gamma_{R, j \leftarrow i} \int_{\mathfrak{T}}^t \mathbf{p}_i(t') dt' \right). \quad (23)$$

Here, $F'_{j \leftarrow i}(\mathfrak{T})$ stands for the numerical integration of (16) in the interval $[\tau; \mathfrak{T}]$ and $\mathbf{1}_{\mathbb{D}}(i)$ is the indicator function [74] of $\mathbb{D} \subset \mathbb{K}$ which is unity for $i \in \mathbb{D}$ and zero otherwise. If $i \in \mathbb{D}$ and $\Gamma_{R, j \leftarrow i} \neq 0$ then the integral $\int_{\mathfrak{T}}^{\infty} \mathbf{p}_i(t') dt'$ is finite because $\mathbf{p}_i(t')$ decreases exponentially toward zero. Otherwise the term in parentheses in (23) vanishes. The integral (14) ($k = R$) is solved analogously.

VIII. CONCLUSION

X-ray FELs such as LCLS, SACLA, SwissFEL, or XFEL offer novel prospects for atomic physics in intense and ultrafast x rays. For the understanding of experiments at FELs, a thorough knowledge of the atomic electronic structure of the samples is essential. In this

work, we lay the foundation for its theoretical treatment with GRASP2K and electronic and radiative transitions as well as photoionization cross sections with RATIP in terms of the CAESR program that processes all nonrelativistic cationic configurations of an atom. The time-dependent quantum dynamics of the interaction of x rays with an atom is described in rate equation approximation. First, plain rate equations are formulated which contain only the cross sections and decay widths from CAESR. Second, modified rate equations are developed that treat additionally double Auger decay of a K -shell vacancy in Ne^+ and photoionization shake off for neutral neon. A detailed path analysis is devised to unravel the mechanisms that produce certain atomic configurations by x-ray absorption and decay. Specifically, the configurations and transitions among them can be arranged in terms of a graph. The interaction with the x rays is then characterized by paths from the neutral atom to a cationic configuration. The transitions in the paths are classified in terms of an alphabet which allows us to assign a string to a path, i.e., words of a formal language. We find that a sequential few-photon absorption is the prevailing mechanism as proposed before. From the solution of the rate equations, we derive easily experimentally accessible quantities, the ion yields and photon yields. We obtain theoretical results for neon atoms in LCLS x rays and reanalyze previous experimental data. We find that the plain rate equations do not provide a satisfactory description of the ion yields of neon, not even below the K -shell ionization threshold, a fact that has been overlooked in previous investigations. Instead, the modified rate equations are required which lead to an overall good agreement apart from charge states for certain photon energies which are significantly populated also by inner-shell resonant absorption. Photon yields from XUV and x-ray fluorescence are predicted and shown to provide more detailed information about the interacting atom than ion yields. We discover that inaccuracies in those Auger decay widths employed in previous studies have only a minor influence on ion and photon yields because of the prevailing mechanism of sequential photon absorption with only a minor contribution of double core holes.

Rich prospects for novel research are enabled by our study. With our program CAESR, other atoms can be ex-

amined and more detailed knowledge of the interaction with x rays can be gained. The foundation of CAESR on state-of-the-art relativistic multiconfiguration methods for atoms provides a solid basis to describe further processes in configuration approximation such as double Auger decay, photoionization shake off, and resonances. Our approach even allows one to go beyond the configuration approximation and to consider also fine-structure-resolved atomic states and transitions. For the ion yields of neon, there is still not always good agreement between the theoretical prediction and the experimental data potentially due to, yet unknown, many-electron effects in neon cations. Future investigations of such effects are very important to ensure that our understanding of the underlying physics is complete. In principle, our improved theory for the interaction of neon with x rays allows one an accurate determination of the actual pulse energy at the sample, a quantity which is still not very well known in LCLS experiments due to uncertainties in the pulse diagnostics and losses in the x-ray optics. Namely, the experimental ion yield of singly ionized neon—determined only from singly and doubly ionized neon—should match the theoretical value, if all other experimental parameters are accurately determined because our theoretical understanding of the population of these two charge states is accurate. However, our comparisons between theory and experiment reveal that this is not the case to date. Photon yields offer exciting novel possibilities for future examinations complementary to Auger electron yields. Specifically, the combined measurement of XUV and x-ray spectra facilitate one to unravel at least some the configurations populated by the absorption of x rays and the ensuing Auger decay processes.

ACKNOWLEDGMENTS

We thank Jochen Schirmer for a critical reading of the manuscript. N.B. and R.O. acknowledge support from the DOE, Sc, BES, DCSGB under grant No. DE-SC0012376. This research has been funded by the German Federal Ministry for Education and Research (BMBF) under Contract No. 05K16SJA.

-
- [1] Richard Neutze, Remco Wouts, David van der Spoel, Edgar Weckert, and Janos Hajdu, “Potential for biomolecular imaging with femtosecond x-ray pulses,” *Nature* **406**, 752–757 (2000).
 - [2] Bernhard W. Adams, Christian Buth, Stefano M. Cavalletto, Jörg Evers, Zoltán Harman, Christoph H. Keitel, Adriana Pálffy, Antonio Picón, Ralf Röhlsberger, Yuri Rostovtsev, and Kenji Tamasaku, “X-ray quantum optics,” *J. Mod. Opt.* **60**, 2–21 (2013).
 - [3] J. Arthur, P. Anfinrud, P. Audebert, K. Bane, I. Ben-

Zvi, V. Bharadwaj, R. Bionta, P. Bolton, M. Borland, P. H. Bucksbaum, R. C. Cauble, J. Clendenin, M. Cornacchia, G. Decker, P. Den Hartog, S. Dierker, D. Dowell, D. Dungan, P. Emma, I. Evans, G. Faigel, R. Falcone, W. M. Fawley, M. Ferrario, A. S. Fisher, R. R. Freeman, J. Frisch, J. Galayda, J.-C. Gauthier, S. Gierman, E. Gluskin, W. Graves, J. Hajdu, J. Hastings, K. Hodgson, Z. Huang, R. Humphry, P. Ilinski, D. Imre, C. Jacobsen, C.-C. Kao, K. R. Kase, K.-J. Kim, R. Kirby, J. Kirz, L. Klaisner, P. Krejčík, K. Kulan-

- der, O. L. Landen, R. W. Lee, C. Lewis, C. Limborg, E. I. Lindau, A. Lumpkin, G. Materlik, S. Mao, J. Miao, S. Mochrie, E. Moog, S. Milton, G. Mulhollan, K. Nelson, W. R. Nelson, R. Neutze, A. Ng, D. Nguyen, H.-D. Nuhn, D. T. Palmer, J. M. Paterson, C. Pellegrini, S. Reiche, M. Renner, D. Riley, C. V. Robinson, S. H. Rokni, S. J. Rose, J. Rosenzweig, R. Ruland, G. Ruocco, D. Saenz, S. Sasaki, D. Sayre, J. Schmerge, D. Schneider, C. Schroeder, L. Serafini, F. Sette, S. Sinha, D. van der Spoel, B. Stephenson, G. Stupakov, M. Sutton, A. Szöke, R. Tatchyn, A. Toor, E. Trakhtenberg, I. Vasserman, N. Vinokurov, X. J. Wang, D. Waltz, J. S. Wark, E. Weckert, Wilson-Squire Group, H. Winick, M. Woodley, A. Wootton, M. Wulff, M. Xie, R. Yotam, L. Young, and A. Zewail, *Linac Coherent Light Source (LCLS): Conceptual Design Report*, Tech. Rep. SLAC-R-593, UC-414 (Stanford Linear Accelerator Center (SLAC), Menlo Park, California, USA, 2002).
- [4] P. Emma, R. Akre, J. Arthur, R. Bionta, C. Bostedt, J. Bozek, A. Brachmann, P. Bucksbaum, R. Coffee, F.-J. Decker, Y. Ding, D. Dowell, S. Edstrom, J. Fisher, A. Frisch, S. Gilevich, J. Hastings, G. Hays, Ph. Hering, Z. Huang, R. Iverson, H. Loos, M. Messerschmidt, A. Miahnahri, S. Moeller, H.-D. Nuhn, G. Pile, D. Ratner, J. Rzepiela, D. Schultz, T. Smith, P. Stefan, H. Tompkins, J. Turner, J. Welch, W. White, J. Wu, G. Yocky, and J. Galayda, “First lasing and operation of an ångstrom-wavelength free-electron laser,” *Nature Photon.* **4**, 641–647 (2010).
- [5] Tetsuya Ishikawa, Hideki Aoyagi, Takao Asaka, Yoshihiro Asano, Noriyoshi Azumi, Teruhiko Bizen, Hiroyasu Ego, Kenji Fukami, Toru Fukui, Yukito Furukawa, Shunji Goto, Hirofumi Hanaki, Toru Hara, Teruaki Hasegawa, Takaki Hatsui, Atsushi Higashiya, Toko Hirono, Naoyasu Hosoda, Miho Ishii, Takahiro Inagaki, Yuichi Inubushi, Toshiro Itoga, Yasumasa Joti, Masahiro Kago, Takashi Kameshima, Hiroaki Kimura, Yoichi Kirihaara, Akio Kiyomichi, Toshiaki Kobayashi, Chikara Kondo, Togo Kudo, Hirokazu Maesaka, Xavier M. Marechal, Takemasa Masuda, Shinichi Matsubara, Takahiro Matsumoto, Tomohiro Matsushita, Sakuo Matsui, Mitsuru Nagasono, Nobuteru Nariyama, Haruhiko Ohashi, Toru Ohata, Takashi Ohshima, Shun Ono, Yuji Otake, Choji Saji, Tatsuyuki Sakurai, Takahiro Sato, Kei Sawada, Takamitsu Seike, Katsutoshi Shirasawa, Takashi Sugimoto, Shinsuke Suzuki, Sunao Takahashi, Hideki Takebe, Kunikazu Takeshita, Kenji Tamasaku, Hitoshi Tanaka, Ryotaro Tanaka, Takashi Tanaka, Tadashi Togashi, Kazuaki Togawa, Atsushi Tokuhisa, Hiromitsu Tomizawa, Kensuke Tono, Shukui Wu, Makina Yabashi, Mitsuhiro Yamaga, Akihiro Yamashita, Kenichi Yanagida, Chao Zhang, Tsumoru Shintake, Hideo Kitamura, and Noritaka Kumagai, “A compact X-ray free-electron laser emitting in the sub-ångstrom region,” *Nat. Photon.* **6**, 540–544 (2012).
- [6] Romain Ganter, ed., *SwissFEL Conceptual Design Report*, PSI Bericht Nr. 10-04 (Paul Scherrer Institut (PSI), Villigen, Switzerland, 2012) http://www.psi.ch/swissfel/CurrentSwissFELPublicationsEN/SwissFEL_CDR_V2_0.23.04.12_small.pdf.
- [7] Massimo Altarelli, Reinhard Brinkmann, Majed Cherqui, Winfried Decking, Barry Dobson, Stefan Düsterer, Gerhard Grübel, Walter Graeff, Heinz Graafsma, Janos Hajdu, Jonathan Marangos, Joachim Pflüger, Harald Redlin, David Riley, Ian Robinson, Jörg Rossbach, Andreas Schwarz, Kai Tiedtke, Thomas Tschentscher, Ivan Vartanians, Hubertus Wabnitz, Hans Weise, Riko Wichmann, Karl Witte, Andreas Wolf, Michael Wulff, and Mikhail Yurkov, eds., *XFEL: The European X-Ray Free-Electron Laser - Technical Design Report*, DESY 2006-097 (DESY XFEL Project Group, Deutsches Elektronen-Synchrotron (DESY), Notkestraße 85, 22607 Hamburg, Germany, 2006).
- [8] Jens Als-Nielsen and Des McMorro, *Elements of Modern X-Ray Physics* (John Wiley & Sons, New York, 2001).
- [9] Matthias Hoener, Li Fang, Oleg Kornilov, Oliver Gessner, Stephen T. Pratt, Markus Gühr, Elliot P. Kanter, Cosmin Blaga, Christoph Bostedt, John D. Bozek, Philip H. Bucksbaum, Christian Buth, Mau Chen, Ryan Coffee, James Cryan, Louis DiMauro, Michael Glowina, Erik Hosler, Edwin Kukk, Stephen R. Leone, Brian McFarland, Marc Messerschmidt, Brendan Murphy, Vladimir Petrovic, Daniel Rolles, and Nora Berrah, “Ultraintense x-ray induced ionization, dissociation, and frustrated absorption in molecular nitrogen,” *Phys. Rev. Lett.* **104**, 253002 (2010).
- [10] Li Fang, Matthias Hoener, Oliver Gessner, Francesco Tarantelli, Stephen T. Pratt, Oleg Kornilov, Christian Buth, Markus Gühr, Elliot P. Kanter, Christoph Bostedt, John D. Bozek, Philip H. Bucksbaum, Mau Chen, Ryan Coffee, James Cryan, Michael Glowina, Edwin Kukk, Stephen R. Leone, and Nora Berrah, “Double core hole production in N₂: Beating the Auger clock,” *Phys. Rev. Lett.* **105**, 083005 (2010), arXiv:1303.1429.
- [11] James P. Cryan, James M. Glowina, Jakob Andreasson, Ali Belkacem, Nora Berrah, Cosmin I. Blaga, Christoph Bostedt, John Bozek, Christian Buth, Louis F. DiMauro, Li Fang, Oliver Gessner, Markus Guehr, Janos Hajdu, Markus P. Hertlein, Matthias Hoener, Oleg Kornilov, Jonathan P. Marangos, Anne M. March, Brian K. McFarland, Hamed Merdji, Vladimir S. Petrović, Chandra Raman, Dipanwita Ray, David Reis, Francesco Tarantelli, Mariano Trigo, James L. White, William White, Linda Young, Philip H. Bucksbaum, and Ryan N. Coffee, “Auger electron angular distribution of double core hole states in the molecular reference frame,” *Phys. Rev. Lett.* **105**, 083004 (2010).
- [12] L. Young, E. P. Kanter, B. Krässig, Y. Li, A. M. March, S. T. Pratt, R. Santra, S. H. Southworth, N. Rohringer, L. F. DiMauro, G. Doumy, C. A. Roedig, N. Berrah, L. Fang, M. Hoener, P. H. Bucksbaum, J. P. Cryan, S. Ghimire, J. M. Glowina, D. A. Reis, J. D. Bozek, C. Bostedt, and M. Messerschmidt, “Femtosecond electronic response of atoms to ultra-intense x-rays,” *Nature* **466**, 56–61 (2010).
- [13] Christian Buth, Ji-Cai Liu, Mau Hsiung Chen, James P. Cryan, Li Fang, James M. Glowina, Matthias Hoener, Ryan N. Coffee, and Nora Berrah, “Ultrafast absorption of intense x rays by nitrogen molecules,” *J. Chem. Phys.* **136**, 214310 (2012), arXiv:1201.1896.
- [14] Li Fang, Timur Osipov, Brendan Murphy, Francesco Tarantelli, Edwin Kukk, James Cryan, Philip H. Bucksbaum, Ryan N. Coffee, Mau Chen, Christian Buth, and Nora Berrah, “Multiphoton ionization as a clock to reveal molecular dynamics with intense short x-ray free electron laser pulses,” *Phys. Rev. Lett.* **109**, 263001 (2012), arXiv:1301.6459.

- [15] Ji-Cai Liu, Nora Berrah, Lorenz S. Cederbaum, James P. Cryan, James M. Glownia, Kenneth J. Schafer, and Christian Buth, “Rate equations for nitrogen molecules in ultrashort and intense x-ray pulses,” *J. Phys. B* **49**, 075602 (2016), arXiv:1508.05223.
- [16] Christian Buth, “Nonlinearity in the sequential absorption of multiple photons,” submitted (2017), arXiv:1612.07105.
- [17] G. Doumy, C. Roedig, S.-K. Son, C. I. Blaga, A. D. DiChiara, R. Santra, N. Berrah, C. Bostedt, J. D. Bozek, P. H. Bucksbaum, J. P. Cryan, L. Fang, S. Ghimire, J. M. Glownia, M. Hoener, E. P. Kanter, B. Krässig, M. Kuebel, M. Messerschmidt, G. G. Paulus, D. A. Reis, N. Rohringer, L. Young, P. Agostini, and L. F. DiMauro, “Nonlinear atomic response to intense ultrashort x rays,” *Phys. Rev. Lett.* **106**, 083002 (2011).
- [18] J. Hofbrucker, A. V. Volotka, and S. Fritzsche, “Relativistic calculations of the nonresonant two-photon ionization of neutral atoms,” *Phys. Rev. A* **94**, 063412 (2016).
- [19] Nina Rohringer and Robin Santra, “Resonant Auger effect at high x-ray intensity,” *Phys. Rev. A* **77**, 053404 (2008); “Publisher’s Note: Resonant Auger effect at high x-ray intensity [Phys. Rev. A **77**, 053404 (2008)],” *Phys. Rev. A* **77**, 059903(E) (2008).
- [20] E. P. Kanter, B. Krässig, Y. Li, A. M. March, P. Ho, N. Rohringer, R. Santra, S. H. Southworth, L. F. DiMauro, G. Doumy, C. A. Roedig, N. Berrah, L. Fang, M. Hoener, P. H. Bucksbaum, S. Ghimire, D. A. Reis, J. D. Bozek, C. Bostedt, M. Messerschmidt, and L. Young, “Unveiling and driving hidden resonances with high-fluence, high-intensity x-ray pulses,” *Phys. Rev. Lett.* **107**, 233001 (2011).
- [21] Stefano M. Cavaletto, Christian Buth, Zoltán Harman, Elliot P. Kanter, Stephen H. Southworth, Linda Young, and Christoph H. Keitel, “Resonance fluorescence in ultrafast and intense x-ray free electron laser pulses,” *Phys. Rev. A* **86**, 033402 (2012), arXiv:1205.4918.
- [22] Nina Rohringer and Richard London, “Atomic inner-shell x-ray laser pumped by an x-ray free-electron laser,” *Phys. Rev. A* **80**, 013809 (2009); “Erratum: Atomic inner-shell x-ray laser pumped by an x-ray free-electron laser [Phys. Rev. A **80**, 013809 (2009)],” *Phys. Rev. A* **82**, 049902(E) (2010).
- [23] Nina Rohringer, Duncan Ryan, Richard A. London, Michael Purvis, Felicie Albert, James Dunn, John D. Bozek, Christoph Bostedt, Alexander Graf, Randal Hill, Stefan P. Hau-Riege, and Jorge J. Rocca, “Atomic inner-shell x-ray laser at 1.46 nm pumped by an x-ray free electron laser,” *Nature* **481**, 488–491 (2012).
- [24] Gábor Darvasi, Christoph H. Keitel, and Christian Buth, “Optical control of an atomic inner-shell x-ray laser,” *Phys. Rev. A* **89**, 013823 (2014), arXiv:1303.2187.
- [25] Christian Buth, Markus C. Kohler, Joachim Ullrich, and Christoph H. Keitel, “High-order harmonic generation enhanced by xuv light,” *Opt. Lett.* **36**, 3530–3532 (2011), arXiv:1012.4930.
- [26] Markus C. Kohler, Carsten Müller, Christian Buth, Alexander B. Voitkiv, Karen Z. Hatsagortsyan, Joachim Ullrich, Thomas Pfeifer, and Christoph H. Keitel, “Electron correlation and interference effects in strong-field processes,” in *Multiphoton Processes and Attosecond Physics*, Springer Proceedings in Physics, Vol. 125, edited by Kaoru Yamanouchi and Katsumi Mi-dorikawa (Springer, Berlin, Heidelberg, 2012) pp. 209–217, arXiv:1111.3555.
- [27] Christian Buth, Feng He, Joachim Ullrich, Christoph H. Keitel, and Karen Zaveni Hatsagortsyan, “Attosecond pulses at kiloelectronvolt photon energies from high-order harmonic generation with core electrons,” *Phys. Rev. A* **88**, 033848 (2013), arXiv:1203.4127.
- [28] Christian Buth, “High-order harmonic generation with resonant core excitation by ultraintense x rays,” *Eur. Phys. J. D* **69**, 234 (2015), arXiv:1303.1332.
- [29] Stefano M. Cavaletto, Zoltán Harman, Christian Buth, and Christoph H. Keitel, “X-ray frequency combs from optically controlled resonance fluorescence,” *Phys. Rev. A* **88**, 063402 (2013), arXiv:1302.3141.
- [30] Stefano M. Cavaletto, Zoltán Harman, Christian Ott, Christian Buth, Thomas Pfeifer, and Christoph H. Keitel, “Broadband high-resolution x-ray frequency combs,” *Nature Photon.* **8**, 520–523 (2014), arXiv:1402.6652.
- [31] Razib Obaid, Christian Buth, Randolph Beerwerth, Lorenz S. Cederbaum, Stephan Fritzsche, *et al.*, and Nora Berrah, in preparation (2017).
- [32] Nina Rohringer and Robin Santra, “X-ray nonlinear optical processes using a self-amplified spontaneous emission free-electron laser,” *Phys. Rev. A* **76**, 033416 (2007).
- [33] Orlando Ciricosta, Hyun-Kyung Chung, Richard W. Lee, and Justin S. Wark, “Simulations of neon irradiated by intense X-ray laser radiation,” *High Energy Density Phys.* **7**, 111–116 (2011).
- [34] Wenjun Xiang, Cheng Gao, Yongsheng Fu, Jiaolong Zeng, and Jianmin Yuan, “Inner-shell resonant absorption effects on evolution dynamics of the charge state distribution in a neon atom interacting with ultraintense x-ray pulses,” *Phys. Rev. A* **86**, 061401(R) (2012).
- [35] C. Gao, J. Zeng, and J. Yuan, “Effects of direct double Auger decay on the population dynamics of neon irradiated by ultraintense x-ray pulses,” *Contrib. Plasma Phys.* **55**, 123–127 (2015).
- [36] Yongqiang Li, Cheng Gao, Wenpu Dong, Jiaolong Zeng, Zengxiu Zhao, and Jianmin Yuan, “Coherence and resonance effects in the ultra-intense laser-induced ultrafast response of complex atoms,” *Sci. Rep.* **6**, 18529 (2016).
- [37] Cheng Gao, Jiaolong Zeng, and Jianmin Yuan, “Single- and double-core-hole ion emission spectroscopy of transient neon plasmas produced by ultraintense x-ray laser pulses,” *J. Phys. B* **49**, 044001 (2016).
- [38] C. P. Bhalla, N. O. Folland, and M. A. Hein, “Theoretical *K*-shell Auger rates, transition energies, and fluorescence yields for multiply ionized neon,” *Phys. Rev. A* **8**, 649–657 (1973).
- [39] Sang-Kil Son, Linda Young, and Robin Santra, “Impact of hollow-atom formation on coherent x-ray scattering at high intensity,” *Phys. Rev. A* **83**, 033402 (2011); “Erratum: Impact of hollow-atom formation on coherent x-ray scattering at high intensity [Phys. Rev. A **83**, 033402 (2011)],” *Phys. Rev. A* **83**, 069906(E) (2011).
- [40] D. R. Hartree, “The wave mechanics of an atom with a non-coulomb central field. Part I. Theory and methods,” *Proc. Camb. Phil. Soc.* **24**, 89–110 (1928).
- [41] Attila Szabo and Neil S. Ostlund, *Modern Quantum Chemistry: Introduction to Advanced Electronic Structure Theory*, 1st, revised ed. (McGraw-Hill, New York, 1989).
- [42] See the Supplementary Data for all numerical results discussed in this work. All rate-equation computations are

- done with *Mathematica* [43].
- [43] *Mathematica 11*, Wolfram Research, Inc., 100 Trade Center Drive, Champaign, Illinois 61820-7237, USA (2016), <http://www.wolfram.com>.
 - [44] Ian P. Grant, *Relativistic Quantum Theory of Atoms and Molecules*, Springer Series on Atomic, Optical, and Plasma Physics (Springer, New York, Berlin, Heidelberg, 2007).
 - [45] Charlotte Froese Fischer, Michel Godefroid, Tomas Brage, Per Jönsson, and Gediminas Gaigalas, “Advanced multiconfiguration methods for complex atoms: I. Energies and wave functions,” *J. Phys. B* **49**, 182004 (2016).
 - [46] P. Jönsson, X. He, C. Froese Fischer, and I. P. Grant, “The grasp2K relativistic atomic structure package,” *Comput. Phys. Commun.* **177**, 597–622 (2007).
 - [47] P. Jönsson, G. Gaigalas, J. Bieroń, C. Froese Fischer, and I. P. Grant, “New version: GRASP2K relativistic atomic structure package,” *Comput. Phys. Commun.* **184**, 2197–2203 (2013).
 - [48] Stephan Fritzsche, “The RATIP program for relativistic calculations of atomic transition, ionization and recombination properties,” *Comput. Phys. Commun.* **183**, 1525–1559 (2012).
 - [49] Ming Feng Gu, “The flexible atomic code,” *Can. J. Phys.* **86**, 675–689 (2008).
 - [50] C. P. Bhalla, “Theoretical fluorescence yields for neon,” *Phys. Rev. A* **12**, 122–128 (1975).
 - [51] V. P. Kozyrev (originator), “Graph,” *Encyclopedia of Mathematics* (2016), <http://www.encyclopediaofmath.org/index.php?title=Graph&oldid=38869>. Accessed 15 March 2017.
 - [52] Norio Saito and Isao H. Suzuki, “Shake-off processes in photoionization and Auger transition for rare gases irradiated by soft X-rays,” *Phys. Scr.* **49**, 80–85 (1994).
 - [53] B. Kanngießer, M. Jainz, S. Brünken, W. Benten, Ch. Gerth, K. Godehusen, K. Tiedtke, P. van Kampen, A. Tutay, P. Zimmermann, V. F. Demekhin, and A. G. Kochur, “Simultaneous determination of radiative and nonradiative decay channels in the neon *K* shell,” *Phys. Rev. A* **62**, 014702 (2000).
 - [54] Y. Hikosaka, T. Kaneyasu, P. Lablanquie, F. Penent, E. Shigemasa, and K. Ito, “Multiple Auger decay of the neon 1s-core-hole state studied by multielectron coincidence spectroscopy,” *Phys. Rev. A* **92**, 033413 (2015).
 - [55] M. Ya. Amusia, I. S. Lee, and V. A. Kilin, “Double Auger decay in atoms: Probability and angular distribution,” *Phys. Rev. A* **45**, 4576–4587 (1992).
 - [56] N. M. Kabachnik, S. Fritzsche, A. N. Grum-Grzhimailo, M. Meyer, and K. Ueda, “Coherence and correlations in photoinduced Auger and fluorescence cascades in atoms,” *Phys. Rep.* **451**, 155–233 (2007).
 - [57] K. Ueda, M. Kitajima, A. De Fanis, Y. Tamenori, H. Yamaoka, H. Shindo, T. Furuta, T. Tanaka, H. Tanaka, H. Yoshida, R. Sankari, S. Aksela, S. Fritzsche, and N. M. Kabachnik, “Doppler-free resonant Raman Auger spectroscopy of $\text{Ne}^+ 2s2p^5 3p$ excited states,” *Phys. Rev. Lett.* **90**, 153005 (2003).
 - [58] H. Yoshida, J. Sasaki, Y. Kawabe, Y. Senba, A. De Fanis, M. Oura, S. Fritzsche, I. P. Sazhina, N. M. Kabachnik, and K. Ueda, “Study of second-step Auger transitions in Auger cascades following $1s \rightarrow 3p$ photoexcitation in Ne,” *J. Phys. B* **38**, 465–486 (2005).
 - [59] A. De Fanis, G. Prümper, U. Hergenhahn, E. Kukk, T. Tanaka, M. Kitajima, H. Tanaka, S. Fritzsche, N. M. Kabachnik, and K. Ueda, “Investigation of valence intermultiplet Auger transitions in Ne following 1s photoelectron recapture,” *J. Phys. B* **38**, 2229–2243 (2005).
 - [60] M. Kitajima, H. Yoshida, A. De Fanis, G. Prümper, U. Hergenhahn, E. Kukk, T. Tanaka, K. Nakagawa, H. Tanaka, S. Fritzsche, I. P. Sazhina, N. M. Kabachnik, and K. Ueda, “A study of inner-valence Auger transitions in Ne^+ induced by the resonant Auger decay of photoexcited $\text{Ne } 1s^{-1} np$ states,” *J. Phys. B* **39**, 1299–1322 (2006).
 - [61] In Refs. 12 and 32, the letter “P” was used to indicate single and double photoionization of core electrons in neon.
 - [62] V. A. Uspenskii (originator), “Algorithm,” *Encyclopedia of Mathematics* (2011), <http://www.encyclopediaofmath.org/index.php?title=Algorithm&oldid=18759>. Accessed 02 April 2017.
 - [63] N. M. Nagorny (originator), “Alphabet,” *Encyclopedia of Mathematics* (2016), <http://www.encyclopediaofmath.org/index.php?title=Alphabet&oldid=38525>. Accessed 02 April 2017.
 - [64] N. M. Nagorny (originator), “Word,” *Encyclopedia of Mathematics* (2016), <http://www.encyclopediaofmath.org/index.php?title=Word&oldid=39767>. Accessed 02 April 2017.
 - [65] A. V. Gladkii (originator), “Grammar, formal,” *Encyclopedia of Mathematics* (2011), http://www.encyclopediaofmath.org/index.php?title=Grammar,_formal&oldid=16820. Accessed 03 April 2017.
 - [66] A. V. Gladkii (originator), “Formal language,” *Encyclopedia of Mathematics* (2016), http://www.encyclopediaofmath.org/index.php?title=Formal_language&oldid=37513. Accessed 03 April 2017.
 - [67] Yet puzzling is that basically no Ne^{8+} ion yields were measured but Ne^{9+} and Ne^{10+} . Our theory predicts no noticeable values for Ne^{7+} and higher charge states; neither do the computations of Refs. 33 and 36 for charge states Ne^{8+} and higher.
 - [68] S. Düsterer, P. Radcliffe, C. Bostedt, J. Bozek, A. L. Cavalieri, R. Coffee, J. T. Costello, D. Cubaynes, L. F. DiMauro, Y. Ding, G. Doumy, F. Grüner, W. Helml, W. Schweinberger, R. Kienberger, A. R. Maier, M. Messerschmidt, V. Richardson, C. Roedig, T. Tschentscher, and M. Meyer, “Femtosecond x-ray pulse length characterization at the Linac Coherent Light Source free-electron laser,” *New J. Phys.* **13**, 093024 (2011).
 - [69] L. P. Kuptsov (originator), “Kronecker symbol,” *Encyclopedia of Mathematics* (2016), http://www.encyclopediaofmath.org/index.php?title=Kronecker_symbol&oldid=37525. Accessed 03 April 2017.
 - [70] Christian Buth, *FELLA – the free electron laser atomic, molecular, and optical physics program package*, Theoretische Chemie, Physikalisch-Chemisches Institut, Ruprecht-Karls-Universität Heidelberg, Im Neuenheimer Feld 229, 69120 Heidelberg, Germany (2017), Version 1.4.0, with contributions by Mark Baertschy, Kevin Christ, Chris H. Greene, Hans-Dieter Meyer, Robin Santra, and Thomas Sommerfeld, <http://www.christianbuth.name>.
 - [71] Michael E. Wieser and Tyler B. Coplen, “Atomic weights of the elements 2009 (IUPAC Technical Report),” *Pure Appl. Chem.* **83**, 359–396 (2011).
 - [72] N. J. Stone, *Table of nuclear magnetic dipole and electric*

- quadrupole moments*, INDC(NDS)-0658 (International Atomic Energy Agency (IAEA), Nuclear Data Section, Vienna International Centre, P.O. Box 100, 1400 Vienna, Austria, 2014) <http://www-nds.iaea.org/publications/indc/indc-nds-0594>.
- [73] S. Fritzsche, C. Froese Fischer, and G. Gaigalas, “RELIC: A program for relativistic configuration interaction calculations,” *Comput. Phys. Commun.* **148**, 103–123 (2002).
- [74] A. A. Konyushkov (originator), “Characteristic function of a set,” *Encyclopedia of Mathematics* (2011), http://www.encyclopediaofmath.org/index.php?title=Characteristic_function_of_a_set&oldid=12927. Accessed 29 April 2017.